Supporting Information

Dual Functions of the Anchoring Groups in Self-Assembled Molecules as Effective Hole-Selective Contacts in Inverted Perovskite Solar Cells

Carlos E. Puerto Galvis,[a] José G. Sánchez,[a] Eugenia Martínez-Ferrero,[a] Wenhui Li [a] and Emilio Palomares [a b]**

[a] Institute of Chemical Research of Catalonia (ICIQ-CERCA), Avda. Països Catalans, 16, 43007 Tarragona, Spain.
Corresponding authors, E-mail: wli@iciq.es epalomares@iciq.es

[b] Catalan Institution for Research and Advanced Studies (ICREA), 08010 Barcelona, Spain.

Experimental section

Device fabrication

Prepatterned ITO glass substrates (1.5 cm × 1.5 cm, 15 Ω sq^{-1}) were sequentially cleaned with ethanol and IPA for 15 min. The ITO substrates were dried with N_2 gas and treated with UV−ozone for 20 min before being transferred into a nitrogen glovebox. The SAM solutions were prepared by dissolving the molecules into anhydrous isopropylic alcohol (IPA) to form 0.1 mM concentration. The solutions were heated at 60 °C overnight to increase the dissolution of molecules. The SAM solutions were filtered using a 0.20 μm PTFE filter before deposition. The SAM solutions were dropped onto the ITO substrates and spin-coated at 3000 rpm for 30 s without further annealing. Then, 1.5 M perovskite solution was prepared by mixing FAI, PbI_2, MABr and $PbBr_2$ in DMF: DMSO mixed solvent (4:1 v: v). CsI in DMSO solution (1.5 M) was added to the perovskite precursor to form the final perovskite solution with the chemical formula of $Cs_{0.05}(FA_{0.85}MA_{0.15})_{0.95}Pb(I_{0.85}Br_{0.15})_3$ and $Cs_{0.05}(FA_{0.99}MA_{0.01})_{0.95}Pb(I_{0.99}Br_{0.01})_3$ (with 15 mol % MACl). The perovskite solution was spin-coated onto SAM-based substrates in a two-step procedure at 2000 rpm for 10 s and 4000 pm for 25 s. A 200 μL chlorobenzene was dropped on the spinning substrate at the last 10 s. The samples were then annealed at 100 °C for 30 min. After perovskite deposition, $PC_{61}BM$ was deposited from a chlorobenzene solution (20 mg mL^{-1}) at 1000 rpm for 60 s and then a bathocuproine solution (0.5 mg mL^{-1} in IPA) was spin-coated at 4000 rpm for 40 s. Subsequently, the samples were transferred into a thermal evaporator to deposit of 100 nm Ag layer at low pressure (<10^{-6} bar) forming a defined area of the devices of 0.104 cm^2.

Characterization

The electrochemical characterization of the SAMs bonded to ITO was conducted using a BioLogic SP150e potentiostat in a classical three-electrode configuration by cyclic voltammetry (CV) procedures. The ITO/SAM substrate served as the working electrode, while carbon and platinum wire acted as the reference and counter electrodes, respectively. The supporting electrolyte consisted of 0.1 M tetrabutylammonium hexafluorophosphate ($TBAPF_6$) solution in DMF.

The $J-V$ curves were recorded using a solar simulator (ABET 11000) and a source meter (Keithley 2400). The curves were registered under 1 Sun conditions (100 mW/cm^2, AM 1.5G)

calibrated with a Si-reference cell. The scan rate employed was 100 mV/s. The EQE was measured by quantum efficiency systems from Lasing, S.A. (IPCE-DC, LS1109-232) and a Newport 2936-R power meter unit. Steady-state photoluminescence (PL) and time-resolved photoluminescence (TRPL) spectra were obtained on an Edinburgh Instruments LifeSpec-II apparatus with a 635 nm laser excitation. Contact angle measurements were performed with an optical tensiometer (Attention Theta Flex, Biolin Scientific, Sweden) using a sessile drop analysis. XPS measurements were performed at room temperature with a SPECS PHOIBOS 150 hemispherical analyzer (SPECS GmbH, Berlin, Germany) in a base pressure of $5x10^{-10}$ mbar. XPS used monochromatic Al K alpha radiation (1486.74 eV) as an excitation source operated at 300 W. The energy resolution, as measured by the FWHM of the Ag 3d5/2 peak for a sputtered silver foil, was 0.62 eV. For UPS we used a monochromatic HeI line at 21.2eV. A high-resolution transmission electron microscope (TEM) was performed with the JEOL F200 equipped with EDX at 200 kV operating voltage. The cross-section was prepared in a scanning electron microscopy (SEM) equipped with focused ion beam (FIB). Fourier transform infrared spectroscopy (FTIR) was conducted in BRUKER ALPHA-P spectrometer with liquid solution. The Gaussian view programs were used to obtain the computed molecule electronic static potential (ESP). Geometries optimization and frequency analysis were performed by DFT/B3LYP method with a basic set of 6-31G(d)(p).

Photoinduced charge extraction (CE), transient photovoltage (TPV), and transient photocurrent (TPC) measurements were carried out using a white LED controlled by a programmable power supply and a control box that switched from open- to short-circuit states. All the signals were recorded using a Yokogawa DLM2052 oscilloscope registering drops in voltage. Light perturbation pulses for TPV and TPC were provided by a nanosecond PTI GL-3300 nitrogen laser and using a 580 nm laser pulse wavelength.

Synthesis of molecules CP203, CP204 and CP226

Unless otherwise specified, all chemicals, reagents, and solvents used in the synthesis of SAMs CP203, CP204 and CP226 were obtained from commercial sources in reagent-grade quality and were employed without additional purification. Sensitive reactions were conducted under an argon atmosphere using standard Schlenk techniques (under high-vacuum, $\sim 10^{-2}$ mbar) with solvents that were distilled and dried, unless otherwise noted. The progress of the reactions was monitored by thin-layer chromatography (TLC) using Merck silica gel 60 F254 precoated

plates (0.25 mm) and visualized with UV lamp. All workup and purification procedures were carried out using reagents and solvents of analytical grade. Flash column chromatography was performed on silica gel (Aldrich, 230-400 mesh). Organic solutions were concentrated under reduced pressure on a Büchi rotatory evaporator. Unless otherwise stated, reactions were carried out under argon atmosphere. Yields refer to purified compounds unless otherwise noted. ^{1}H and ^{13}C NMR spectra were recorded at 298 K on Bruker Avance 400 Ultrashield or Bruker Avance 500 Ultrashield apparatuses. Coupling constants (*J*) are quoted in hertz (Hz). Multiplicity is reported with the following abbreviations: s = singlet, brs = broad singlet, d = doublet, t = triplet, q = quartet, dt = doublet of triplets, td = triplet of doublets, tt = triplet of triplets, sp = septet, m = multiplet, app = apparent. Melting points were measured using open glass capillaries in a Büchi B540 apparatus. Infrared spectra were recorded on a Bruker Tensor 27. Mass spectra were recorded on a Waters LCT Premier spectrometer. Gas chromatography-mass spectrometry
(GC-MS) was carried out in Agilent 7890B - 5877A MSD.

The synthesis of compound (*E*)-3-(4-(3,6-bis(2,4-dimethoxyphenyl)-9*H*-carbazol-9-yl)phenyl)-2-cyanoacrylic acid **CP203** was performed according to the synthetic route described in Scheme S1.

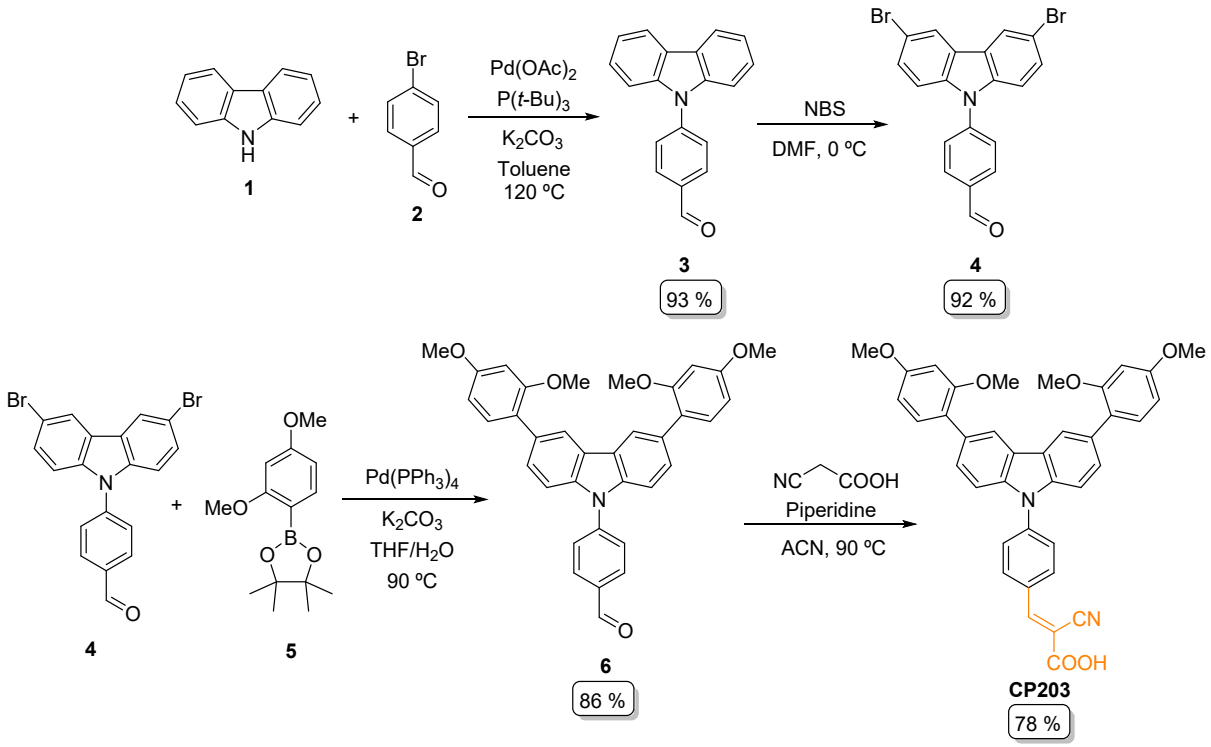

Scheme S1. Synthetic route for SAM **CP203**.

*4-(9H-carbazol-9-yl)benzaldehyde **3**:*

In a 50 mL vial, palladium acetate (126 mg, 10 mol %) and potassium carbonate (2.313 g, 16.74 mmol) were dissolved in anhydrous toluene (15 mL) under inert atmosphere. Then, tri-*tert*-butylphosphine (203 uL, 15 mol %) was added in one portion and the reaction was stirred at room temperature for 15 min before the addition of carbazole **1** (1 g, 5.59 mmol) and 4-bromobenzaldehyde **2** (1.239 g, 6.69 mmol) and the reaction was stirred at 120 ºC for 24 h. The reaction mixture was cooled to room temperature and then was filtered through a pad of celite, after washing with ethyl acetate, the solvent was eliminated under reduced pressure, the crude was purified through column chromatography (Hex/THF: 15/1) to give 4-(9*H*-carbazol-9-yl)benzaldehyde **3** (1.41 g, 5.20 mmol) as a white solid in 93 % yield. $\boldsymbol{R_f}$: 0.3 (Hex/THF: 15/1); **^{1}H NMR** (400 MHz, $CDCl_3$) $\delta_{(ppm)}$: 10.12 (s, 1H), 8.17 – 8.12 (m, 4H), 7.82 – 7.78 (m, 2H), 7.51 (dt, *J* = 8.3, 0.9 Hz, 2H), 7.47 – 7.42 (m, 2H), 7.34 (ddd, *J* = 8.1, 7.1, 1.1 Hz, 2H); **^{13}C NMR** (101 MHz, $CDCl_3$) $\delta_{(ppm)}$: 191.1, 143.5, 140.2, 134.8, 131.5, 127.0, 126.4, 124.1, 120.9, 120.6, 109.9.

*4-(3,6-dibromo-9H-carbazol-9-yl)benzaldehyde **4**:*

In a 50 mL reactor, 4-(9*H*-carbazol-9-yl)benzaldehyde **3** (1 g, 3.68 mmol) was dissolved in DMF (20 mL) and the reactor was cooled down to 0 ºC using an ice-bath. To the reaction mixture, a solution of *N*-bromosuccinimide (1.64 g, 9.21 mmol) in 10 mL of DMF was added dropwise and the system was stirred overnight. To the reaction mixture was added crushed ice and the precipitate solid was filtered and dried at 60 ºC to give 4-(3,6-dibromo-9*H*-carbazol-9-yl)benzaldehyde **4** (1.57 g, 3.66 mmol) as a beige solid in 92 % yield. **^{1}H NMR** (400 MHz, $CDCl_3$) $\delta_{(ppm)}$: 10.13 (s, 1H), 8.21 (dd, *J* = 1.9, 0.5 Hz, 2H), 8.17 – 8.13 (m, 2H), 7.74 – 7.71 (m, 2H), 7.54 (dd, *J* = 8.7, 1.9 Hz, 2H), 7.34 (d, *J* = 8.7 Hz, 2H); **^{13}C NMR** (101 MHz, $CDCl_3$) $\delta_{(ppm)}$: 190.8, 139.3, 135.4, 131.7, 129.9, 127.0, 124.6, 123.6, 114.0, 111.6. This intermediate was used without further purification in the next step.

*4-(3,6-bis(2,4-dimethoxyphenyl)-9H-carbazol-9-yl)benzaldehyde **6**:*

In a 25 mL vial, 4-(3,6-dibromo-9*H*-carbazol-9-yl)benzaldehyde **4** (0.6 g, 1.39 mmol), 2-(2,4-dimethoxyphenyl)-4,4,5,5-tetramethyl-1,3,2-dioxaborolane **5** (0.92 g, 3.47 mmol), $Pd(PPh_3)_4$ (323 mg, 20 mmol %) and K_2CO_3 (1.15 g, 8.34 mmol) were mixed and purged with argon three times. Then, THF (8 mL) and deionized water (4 mL) were added into the vessel and the reaction was left stirring for 24 hours at 90°C under argon atmosphere. The reaction was then

warmed to room temperature and quenched with brine. The resulting reaction mixture was extracted with EtOAc (3x20mL) and washed with brine and the organic layer was separated, dried with sodium sulphate, filtered and concentrated via rotary evaporation. The crude was purified by column chromatography on silica gel (Hexane/THF: 2/1) to give 4-(3,6-bis(2,4-dimethoxyphenyl)-9*H*-carbazol-9-yl)benzaldehyde **6** (0.65 g, 1.19 mmol) as a yellowish solid in 86 % yield. ***R_f***: 0.4 (Hex/THF: 2/1); **^{1}H NMR** (400 MHz, $CDCl_3$) $\delta_{(ppm)}$: 10.12 (s, 1H), 8.24 (d, *J* = 1.0 Hz, 2H), 8.14 (d, *J* = 8.6 Hz, 2H), 7.86 – 7.83 (m, 2H), 7.60 – 7.57 (m, 2H), 7.54 (d, *J* = 0.7 Hz, 2H), 7.36 (d, *J* = 8.8 Hz, 2H), 6.62 (dd, *J* = 6.4, 2.7 Hz, 4H), 3.88 (s, 6H), 3.83 (s, 6H); **^{13}C NMR** (101 MHz, $CDCl_3$) $\delta_{(ppm)}$: 191.1, 160.2, 157.6, 143.8, 139.3, 134.5, 131.6, 131.5, 131.3, 128.1, 126.7, 124.3, 124.1, 121.4, 109.3, 104.8, 99.2, 55.8, 55.6.

(E)-3-(4-(3,6-bis(2,4-dimethoxyphenyl)-9H-carbazol-9-yl)phenyl)-2-cyanoacrylic acid ***CP203****:*

In a 20 mL vial, 4-(3,6-bis(2,4-dimethoxyphenyl)-9*H*-carbazol-9-yl)benzaldehyde **6** (0.55 g, 1.02 mmol) were dissolved in acetonitrile (10 mL) and cyanoacetic acid (0.128 g, 1.5 mmol) was added in one portion. Then, piperidine (4 drops) was added in one portion at room temperature to be used as the catalyzer. Finally, the mixture was stirred at 90 °C for 12 h. After cooling down to room temperature, the solvent was removed under reduced pressure and the residue was quenched with 30 mL of HCl (5M). The precipitated solid was filtered and washed with water and hexane. The crude solid was purified through column chromatography (DMC/MeOH; 10/1) to obtain the corresponding (*E*)-3-(4-(3,6-bis(2,4-dimethoxyphenyl)-9*H*-carbazol-9-yl)phenyl)-2-cyanoacrylic acid **CP203** (0.48 g, 0.79 mmol) as a yellow solid in 78 % yield. ***R_f***: 0.5 (DCM/EtOH/AcOH: 10/1/4 drops); **^{1}H NMR** (400 MHz, CD_2Cl_2) $\delta_{(ppm)}$: 8.41 (s, 1H), 8.30 (d, *J* = 8.7 Hz, 2H), 8.23 (t, *J* = 1.3 Hz, 2H), 7.86 (d, *J* = 8.7 Hz, 2H), 7.58 (d, *J* = 1.2 Hz, 4H), 7.35 (d, *J* = 8.9 Hz, 2H), 6.62 (dq, *J* = 5.5, 2.5 Hz, 4H), 3.87 (s, 6H), 3.83 (s, 6H). **^{13}C NMR** (101 MHz, CD_2Cl_2) $\delta_{(ppm)}$: 160.6, 157.9, 154.5, 151.8, 142.9, 139.4, 136.2, 133.3, 131.8, 131.8, 128.7, 128.5, 126.9, 125.8, 124.5, 124.1, 121.5, 109.7, 105.2, 99.3, 55.9, 55.8. **HRMS** (ESI): calculated for $C_{38}H_{31}N_2O_6^+$ $[M+H]^+$ m/z: 611.2176; found: 611.2170.

The synthesis of compound (4-(3,6-bis(2,4-dimethoxyphenyl)-9*H*-carbazol-9-yl)phenyl)phosphonic acid **CP204** was performed according to the synthetic route described in Scheme S2.

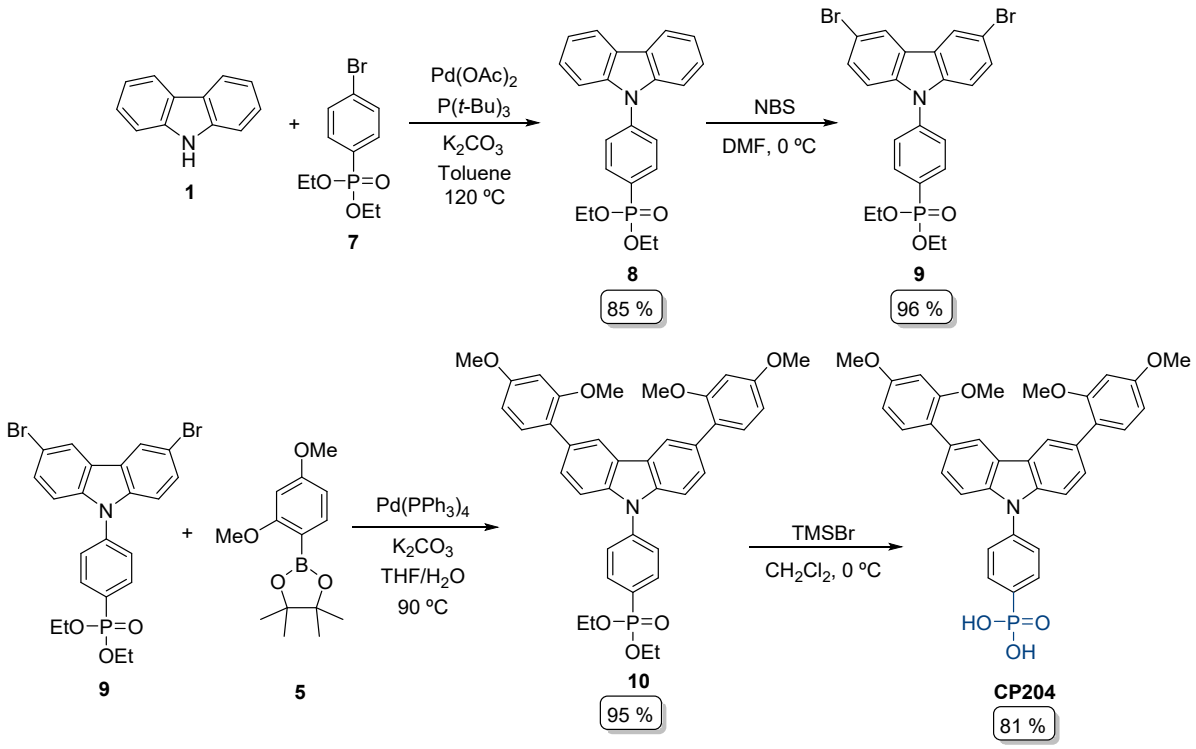

Scheme S2. Synthetic route for SAM **CP204**.

*Diethyl (4-(9H-carbazol-9-yl)phenyl)phosphonate **8**:*

In a 50 mL vial, palladium acetate (67.1 mg, 10 mol %) and potassium carbonate (1.24 g, 8.97 mmol) were dissolved in anhydrous toluene (15 mL) under inert atmosphere. Then, tri-*tert*-butylphosphine (109 uL, 15 mol %) was added in one portion and the reaction was stirred at room temperature for 15 min before the addition of carbazole **1** (0.5 g, 2.99 mmol) and (4-bromophenyl)phosphonate **7** (746 uL, 3.59 mmol)) and the reaction was stirred at 120 ºC for 24 h. The reaction mixture was cooled to room temperature and then was filtered through a pad of celite, after washing with ethyl acetate, the solvent was eliminated under reduced pressure and the crude was triturated with hexane and the solid was filtered and dried to obtain diethyl (4-(9*H*-carbazol-9-yl)phenyl)phosphonate **8** (0.96 g, 2.53 mmol) as a white solid in 85 % yield. ***R*$_f$**: 0.3 (Hex/THF: 2/1); **^{1}H NMR** (400 MHz, $CDCl_3$) $\delta_{(ppm)}$: 8.15 (d, J = 7.7 Hz, 2H), 8.09 – 8.02 (m, 2H), 7.75 – 7.69 (m, 2H), 7.48 (d, J = 8.2 Hz, 2H), 7.45 – 7.40 (m, 2H), 7.34 – 7.29 (m, 2H), 4.31 – 4.15 (m, 4H), 1.41 (t, J = 7.1 Hz, 3H); **^{13}C NMR** (101 MHz, $CDCl_3$) $\delta_{(ppm)}$: 140.3, 133.6, 126.7, 126.3, 123.9, 120.6, 109.8, 62.4, 16.6; **^{31}P NMR** (162 MHz, $CDCl_3$) $\delta_{(ppm)}$: 20.9.

*Diethyl (4-(3,6-dibromo-9H-carbazol-9-yl)phenyl)phosphonate **9**:*

In a 25 mL reactor, diethyl (4-(9*H*-carbazol-9-yl)phenyl)phosphonate **8** (0.5 g, 1.12 mmol) was dissolved in DMF (10 mL) and the reactor was cooled down to 0 ºC using an ice-bath. To the reaction mixture, a solution of *N*-bromosuccinimide (0.5 g, 2.8 mmol) in 5 mL of DMF was added dropwise and the system was stirred overnight. To the reaction mixture was added crushed ice and the precipitate solid was filtered and dried at 60 ºC to give diethyl (4-(3,6-dibromo-9*H*-carbazol-9-yl)phenyl)phosphonate **9** (0.57 g, 1.07 mmol) as a beige solid in 96 % yield. **^{1}H NMR** (400 MHz, $CDCl_3$) $\delta_{(ppm)}$: 8.20 (d, *J* = 2.0 Hz, 2H), 8.06 (dd, *J* = 12.8, 8.0 Hz, 2H), 7.65 – 7.60 (m, 2H), 7.52 (dd, *J* = 8.8, 2.0 Hz, 2H), 7.30 (dd, *J* = 8.7, 2.0 Hz, 2H), 4.31 – 4.14 (m, 4H), 1.40 (t, *J* = 7.0 Hz, 6H); **^{13}C NMR** (101 MHz, $CDCl_3$) $\delta_{(ppm)}$: 139.4, 133.9, 129.79, 126.7, 124.4, 123.5, 113.8, 111.5, 62.6, 16.6; **^{31}P NMR** (162 MHz, $CDCl_3$) $\delta_{(ppm)}$: 20.3. This intermediate was used without further purification in the next step.

*Diethyl (4-(3,6-bis(2,4-dimethoxyphenyl)-9H-carbazol-9-yl)phenyl)phosphonate **10**:*

In a 25 mL vial, diethyl (4-(3,6-dibromo-9*H*-carbazol-9-yl)phenyl)phosphonate **9** (0.6 g, 1.11 mmol), 2-(2,4-dimethoxyphenyl)-4,4,5,5-tetramethyl-1,3,2-dioxaborolane **5** (0.73 g, 2.79 mmol), $Pd(PPh_3)_4$ (258 mg, 20 mmol %) and K_2CO_3 (0.920 g, 6.66 mmol) were mixed and purged with argon three times. Then, THF (8 mL) and deionized water (4 mL) were added into the vessel and the reaction was left stirring for 24 hours at 90°C under argon atmosphere. The reaction was then warmed to room temperature and quenched with brine. The resulting reaction mixture was extracted with EtOAc (3x20mL) and washed with brine and the organic layer was separated, dried with sodium sulphate, filtered and concentrated via rotary evaporation. The crude was purified by column chromatography on silica gel (Hexane/THF: 2/1) to give diethyl (4-(3,6-bis(2,4-dimethoxyphenyl)-9*H*-carbazol-9-yl)phenyl)phosphonate **10** (0.68 g, 1.04 mmol) as a yellowish solid in 95 % yield. R_f: 0.4 (Hex/THF: 2/1); **^{1}H NMR** (400 MHz, $CDCl_3$) $\delta_{(ppm)}$: 8.23 (dd, *J* = 1.8, 0.7 Hz, 2H), 8.06 (dd, *J* = 12.9, 8.4 Hz, 2H), 7.76 (dd, *J* = 8.4, 3.6 Hz, 2H), 7.67 (ddd, *J* = 12.0, 8.3, 1.4 Hz, 2H), 7.57 (dd, *J* = 8.5, 1.7 Hz, 2H), 7.36 (d, *J* = 8.7 Hz, 2H), 6.62 (dd, *J* = 6.6, 2.4 Hz, 4H), 4.29 – 4.16 (m, 4H), 3.88 (s, 6H), 3.83 (s, 6H), 1.41 (t, *J* = 7.3 Hz, 6H); **^{13}C NMR** (101 MHz, $CDCl_3$) $\delta_{(ppm)}$: 160.2, 157.6, 139.5, 133.7, 132.3, 132.0, 131.6, 131.0, 128.5, 128.0, 126.4, 124.1, 121.4, 109.3, 104.8, 99.2, 62.4, 55.8, 55.6, 16.6; **^{31}P NMR** (162 MHz, $CDCl_3$) $\delta_{(ppm)}$: 21.0.

*(4-(3,6-bis(2,4-dimethoxyphenyl)-9H-carbazol-9-yl)phenyl)phosphonic acid **CP204**:*

In a 10 mL vial, diethyl (4-(3,6-bis(2,4-dimethoxyphenyl)-9*H*-carbazol-9-yl)phenyl)phosphonate **10** (0.66 g, 1.02 mmol) was dissolved in DCM (10 mL) at room temperature. Then, TMSBr (800 uL, 5.64 mmol) was added in one portion and the reaction was stirred at room temperature for 36 h. Then, methanol (10 mL) was added to the reaction mixture and the system was stirred for 2 hours before removing the solvent under reduced pressure, the crude was triturated with hexane and diethyl ether and the solid was filtered and dried to obtain the corresponding (4-(3,6-bis(2,4-dimethoxyphenyl)-9*H*-carbazol-9-yl)phenyl)phosphonic acid **CP204** (0.49 g, 0.82 mmol) as a gray solid in 81 % yield. **^{1}H NMR** (400 MHz, CD_2Cl_2) $\delta_{(ppm)}$: 8.13 (m, 4H), 7.73 (m, 2H), 7.39 (m, 4H), 7.18 (d, J = 8.4 Hz, 2H), 6.53 – 6.47 (m, 4H), 3.80 (s, 6H), 3.70 (s, 6H); **^{13}C NMR** (101 MHz, CD_2Cl_2) $\delta_{(ppm)}$: 160.4, 157.8, 139.5, 131.7, 131.4, 128.3, 124.2, 121.4, 109.5, 105.0, 99.2, 55.8, 55.7; **^{31}P NMR** (162 MHz, CD_2Cl_2) $\delta_{(ppm)}$: 24.2. **HRMS** (ESI): calculated for $C_{34}H_{31}NO_7P^+$ $[M+H]^+$ m/z: 597.1832; found: 597.1835.

The synthesis of compound 2-(4-(3,6-bis(2,4-dimethoxyphenyl)-9*H*-carbazol-9-yl)benzylidene)malononitrile **CP226** was performed acoording to the synthetic route described in Scheme S3.

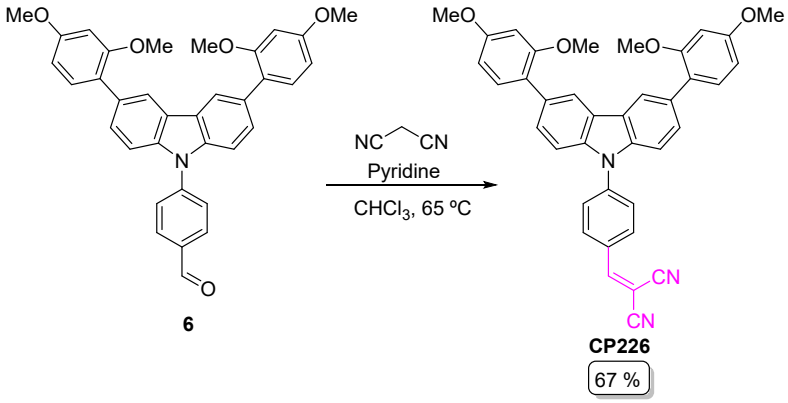

Scheme S3. Synthetic route for SAM **CP226**.

*2-(4-(3,6-bis(2,4-dimethoxyphenyl)-9H-carbazol-9-yl)benzylidene)malononitrile **CP226**:*

In a 20 mL vial, 4-(3,6-bis(2,4-dimethoxyphenyl)-9*H*-carbazol-9-yl)benzaldehyde **6** (0.46 g, 0.858 mmol) were dissolved in chloroform (5 mL) and malononitrile (0.566 g, 8.58 mmol) was added in one portion. Then, pyridine (5 mL) was added in one portion at room temperature and the mixture was stirred at 90 °C for 12 h. After cooling down to room temperature, the residue was extracted with dichloromethane. The organic layer was dried over Na_2SO_4, concentrated

and the crude solid was purified through column chromatography (Hex/THF; 1/1) to obtain the corresponding 2-(4-(3,6-bis(2,4-dimethoxyphenyl)-9*H*-carbazol-9-yl)benzylidene)malononitrile **CP226** (0.34 g, 0.57 mmol) as a yellow solid in 67 % yield. $\boldsymbol{R_f}$: 0.3 (Hex/THF: 2/1 drops); **^{1}H NMR** (400 MHz, $CDCl_3$) $\delta_{(ppm)}$: 8.23 (d, J = 0.8 Hz, 2H), 8.19 – 8.16 (m, 2H), 7.89 – 7.85 (m, 2H), 7.84 (s, 1H), 7.61 – 7.55 (m, 2H), 7.36 (d, J = 9.0 Hz, 0H), 6.98 (d, J = 0.8 Hz, 2H), 6.64 – 6.61 (m, 4H), 3.88 (s, 6H), 3.83 (s, 6H); **^{13}C NMR** (101 MHz, $CDCl_3$) $\delta_{(ppm)}$: 160.3, 158.4, 157.6, 138.9, 135.9, 132.7, 131.9, 131.6, 128.3, 126.6, 125.6, 124.7, 123.9, 121.5, 109.4, 104.8, 99.2, 55.8, 55.6. **HRMS** (ESI): calculated for $C_{38}H_{30}N_3O_4^+$ $[M+H]^+$ m/z: 592.2230; found: 592.2227.

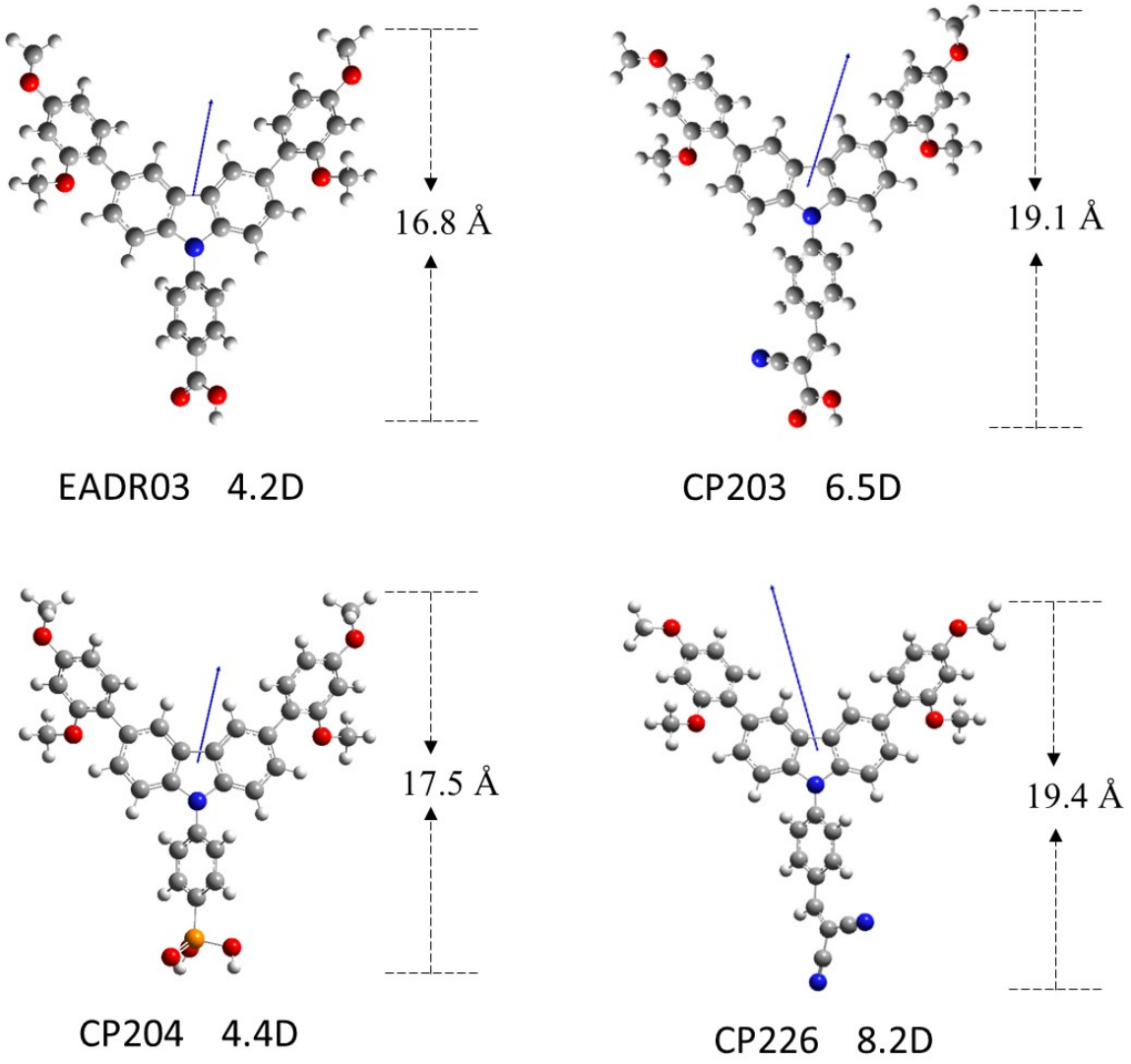

Fig. S1. The molecular structures, calculated dipole moments and molecular heights of EADR03, CP203, CP204 and CP226.

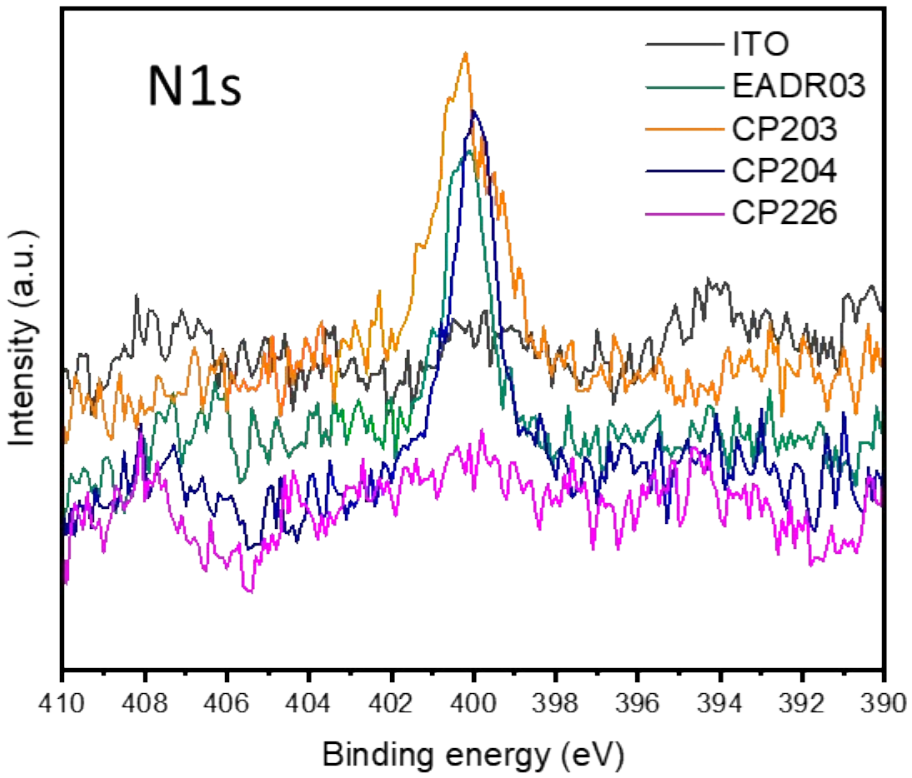

Fig. S2. XPS survey spectra of the N1s region of ITO, ITO/EADR03, ITO/CP203, ITO/CP204 and ITO/CP226.

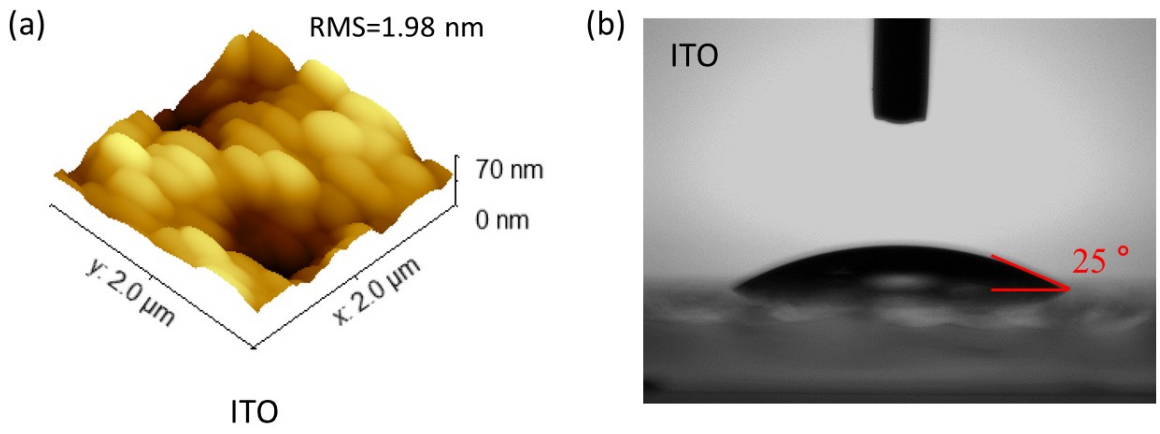

Fig. S3. AFM image (a) and contact angle (b) of ITO surface.

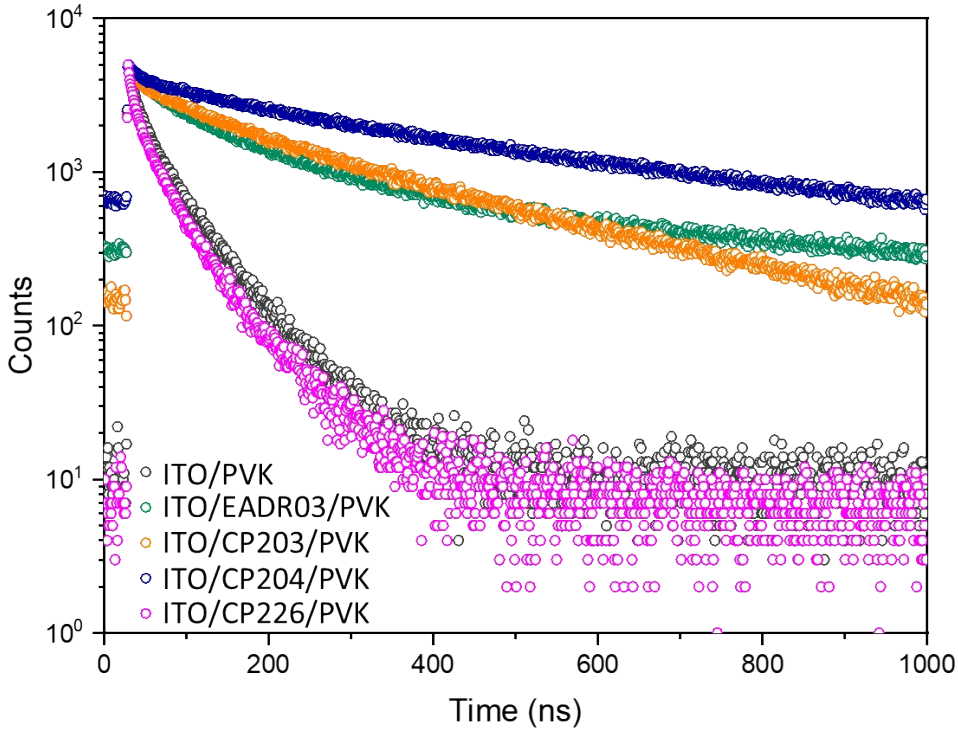

Fig. S4. Time-resolved photoluminescence (TRPL) decays of perovskite deposited on different substrates with excitation from ITO side at 635 nm.

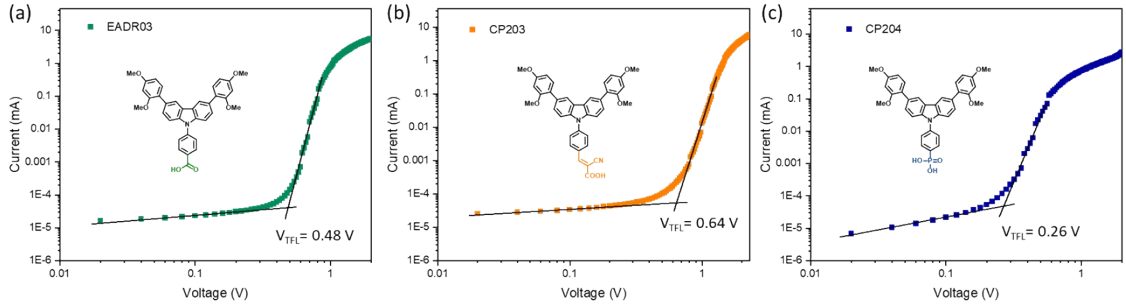

Fig. S5. Space charge limited current (SCLC) plots of hole-only devices based on EADR03, CP203 and CP204 SAMs.

The dark J-V curves of hole-only devices can be divided into three parts, i) the ohmic region, ii) trap-filling limited region with a sharp increase in current, and iii) trap-free child's region. The trap density (n_t) of perovskite films can be calculated from the trap-filling limited voltage (V_{TFL}), which is a transition point of J-V behavior from Ohmic to trap-filling limited region. The caculated equation is as follows:

$$n_t = \frac{2\varepsilon\varepsilon_0 V_{TFL}}{eL^2}$$

Where e is the elementary charge, L is the thickness of perovskite layer, ε_r is the relative dielectric constant of perovskite, and ε_0 is the vacuum permittivity.

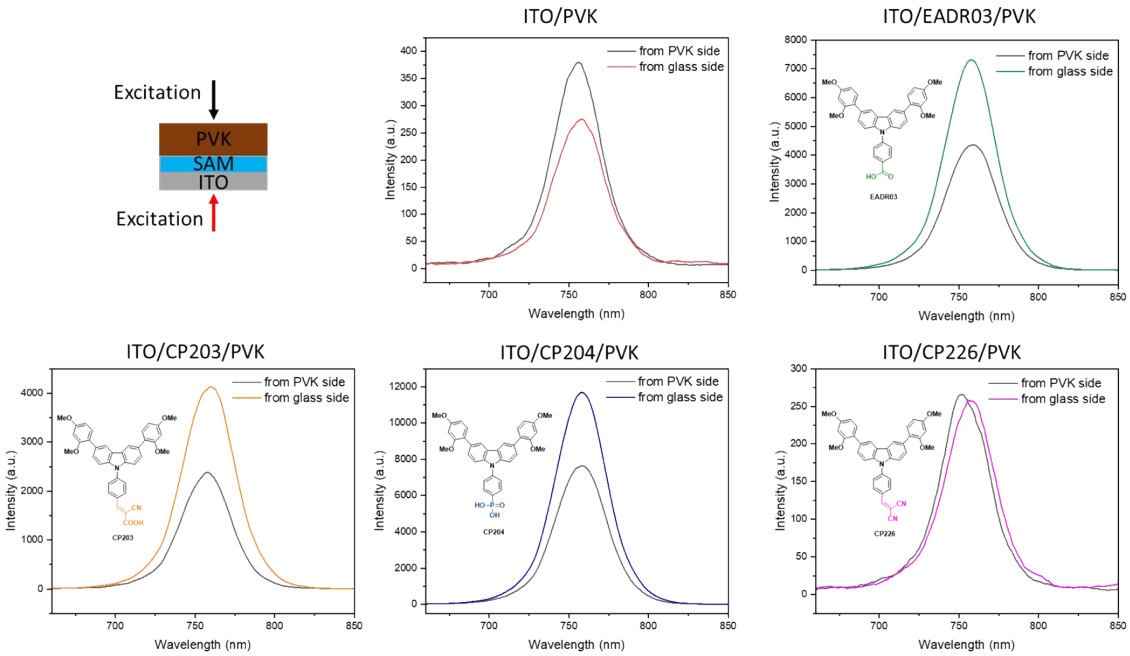

Fig. S6. Steady-state PL spectra of perovskite deposited on ITO and ITO/SAMs substrates with excitation from ITO and perovskite sides by 635 nm laser.

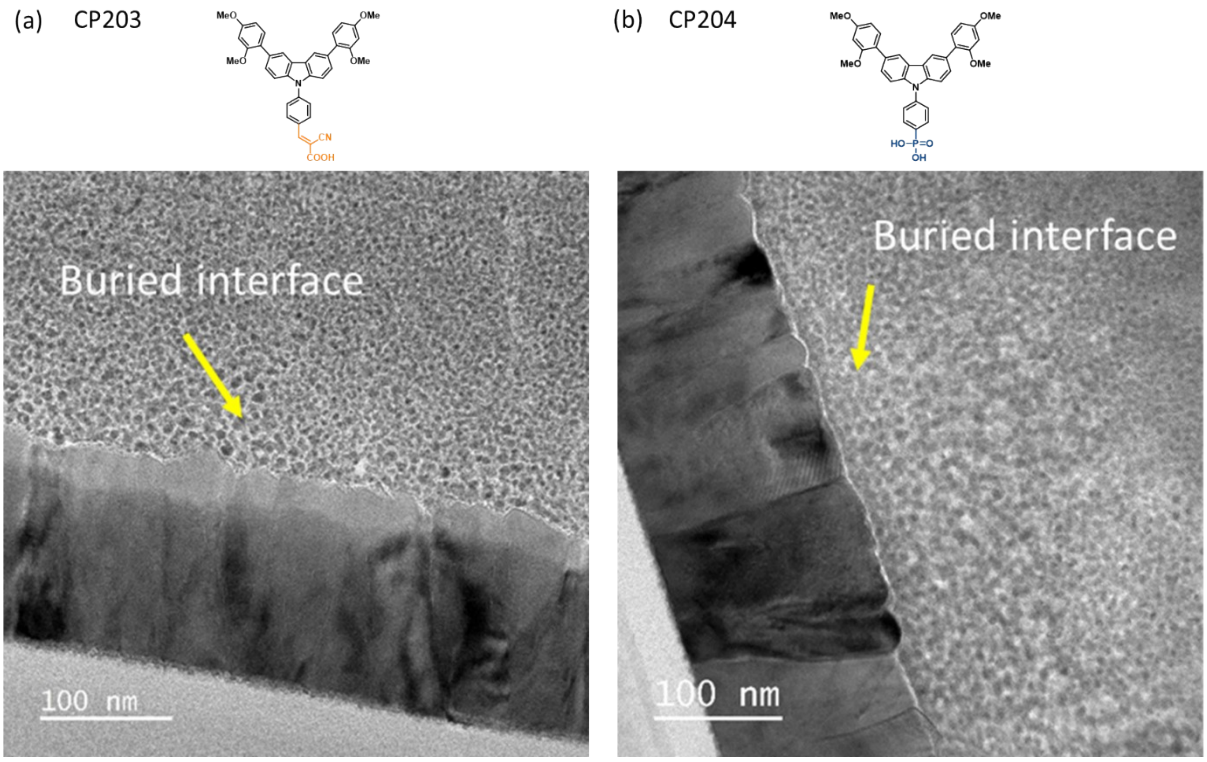

Fig. S7. The high-resolution TEM image of buried interface of ITO/CP203/perovskite (a) and ITO/CP204/perovskite (b).

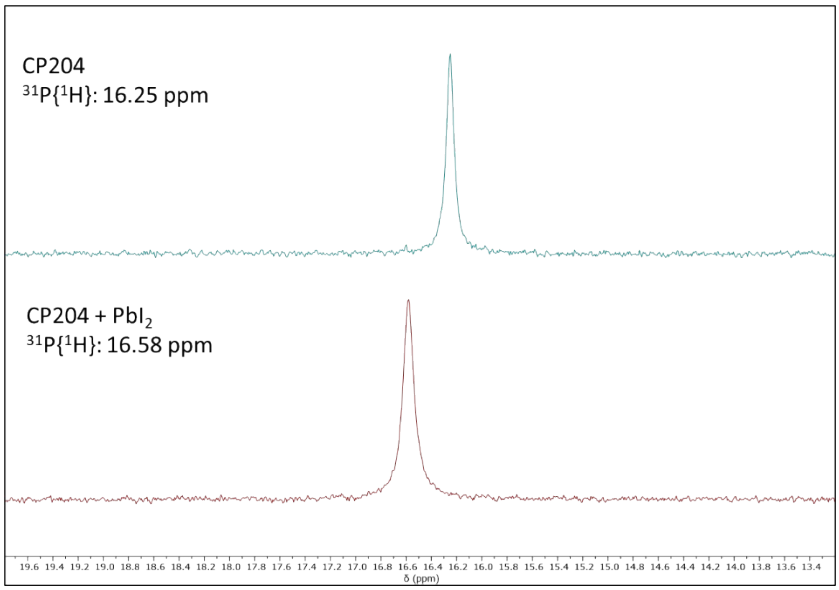

Fig. S8. ^{31}P NMR spectra of CP204 SAM and CP204 with PbI_2 in DMF solution.

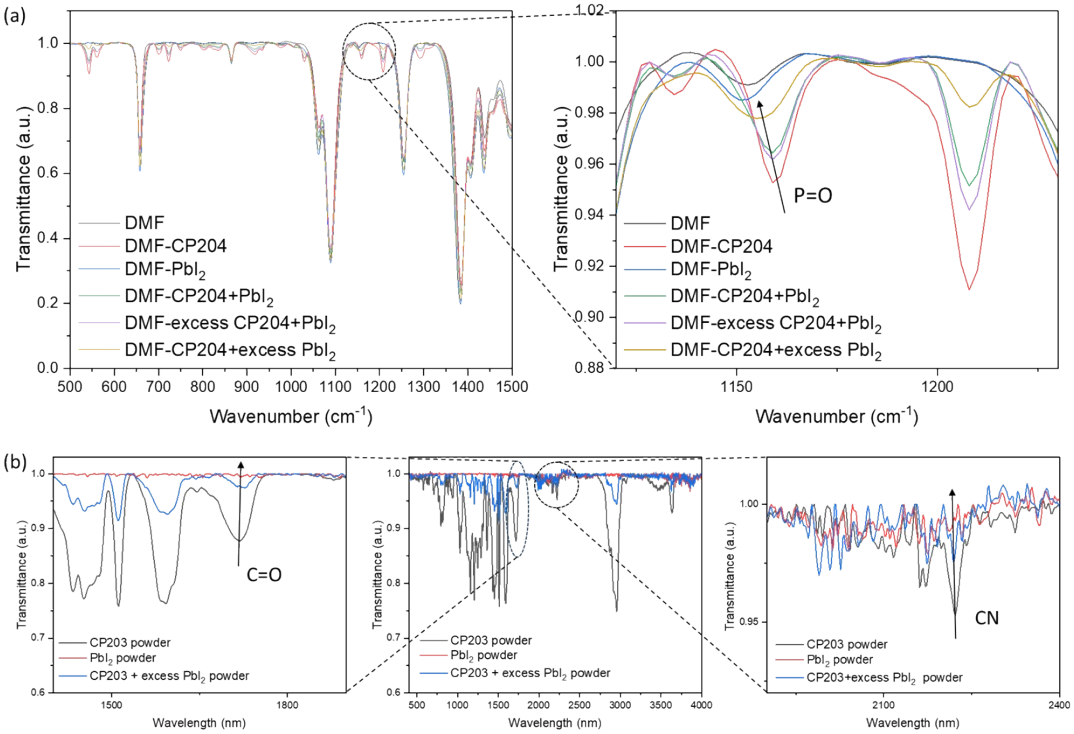

Fig. S9. FTIR spectra of (a) DMF, CP204 in DMF, PbI_2 in DMF, CP204 with PbI_2 in DMF, excess CP204 with PbI_2 in DMF, and CP204 with excess PbI_2 DMF. The peak at 1158 cm^{-1} is assigned to P=O of phosphonic acid. (b) powders of CP203, PbI_2 and CP203 with excess PbI_2. Note: due to the signal interference of DMF solvent, we conducted the measurement with powders of CP203, PbI_2 and mixtures (the mixture is obtained by drying the CP203-PbI_2-DMF solution).

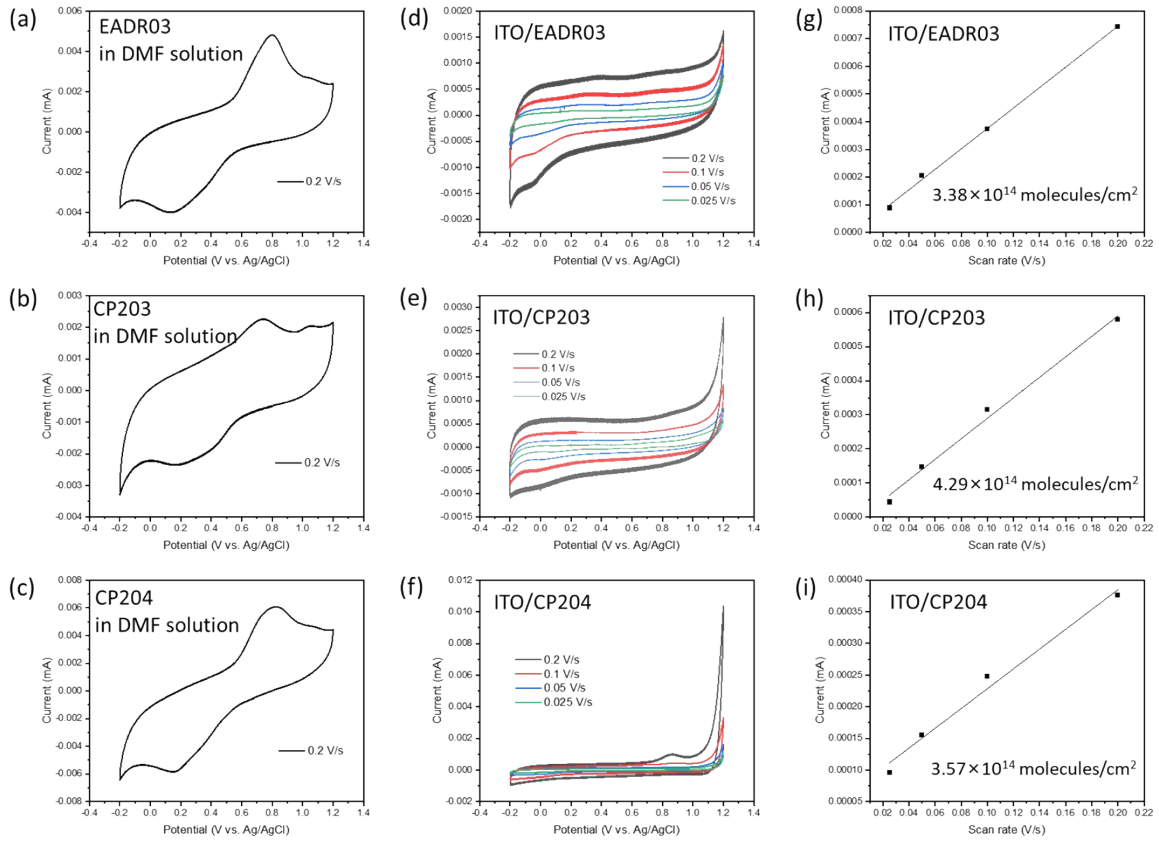

Fig. S10. Cyclic voltammetry of EADR03, CP203 and CP204 SAMs dissolved in DMF (a-c), and of ITO/SAMs under different voltage scan rates and their corresponding peak current vs. scan rate (g-i). 0.1M $TBAPF_6$ was used as electrolyte.

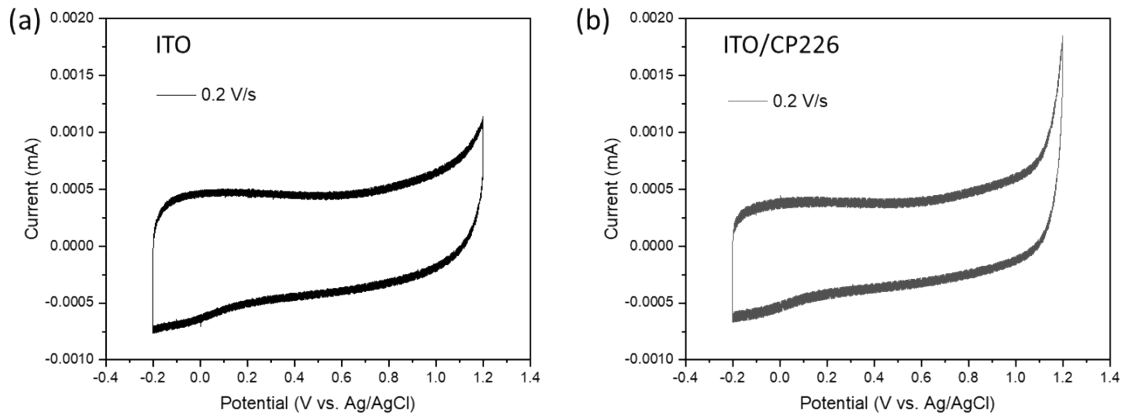

Fig. S11. Cyclic voltammetry of bare ITO (a) and ITO/CP204 (b) at 0.2 V/s scan rate. 0.1M $TBAPF_6$ was used as electrolyte

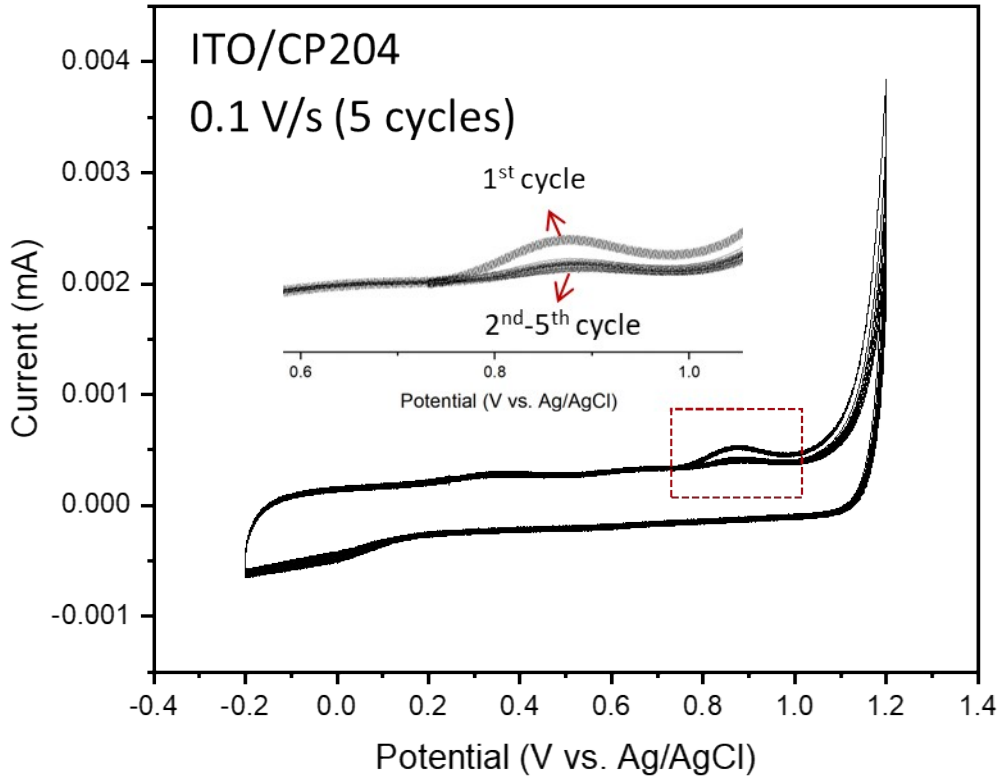

Fig. S12. Cyclic voltammetry of ITO/CP204 during 5 cycles at 0.1 V/s scan rate. 0.1M $TBAPF_6$ was used as electrolyte.

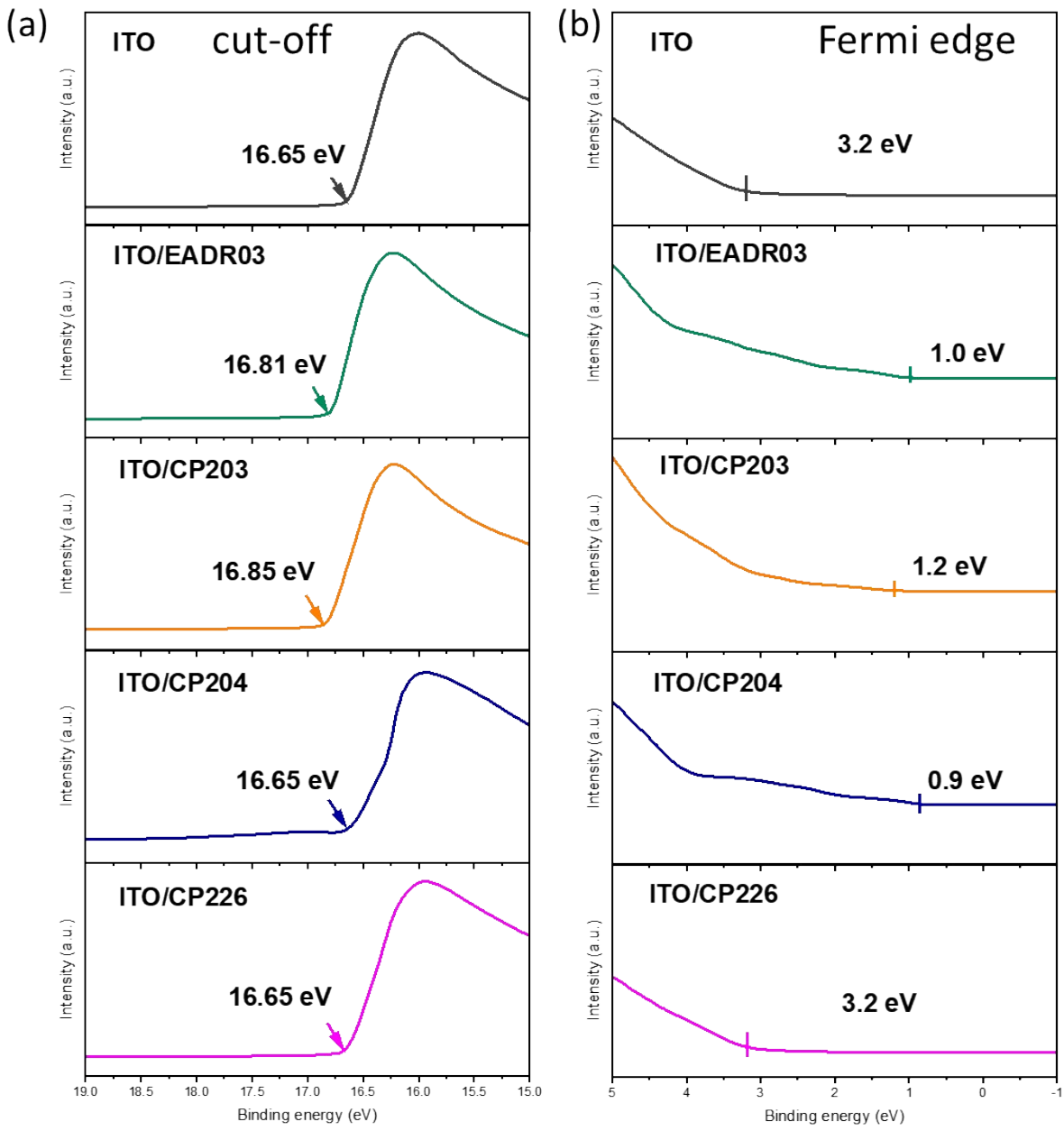

Fig. S13. UPS spectra from ITO and ITO/SAMs substrates, (a) the cut-off energy ($E_{\text{cut-off}}$) region and (b) Fermi edge ($E_{\text{F,edge}}$) region. The Fermi level (E_{F}) is calculated from $E_{\text{F}} = E_{\text{cut-off}}$ (cut-off binding energy) - 21.2 eV (emission energy from He irradiation). The HOMO level of SAMs is calculated from $E_{\text{HOMO}} = E_{\text{F}} - E_{\text{F,edge}}$ (Fermi edge).

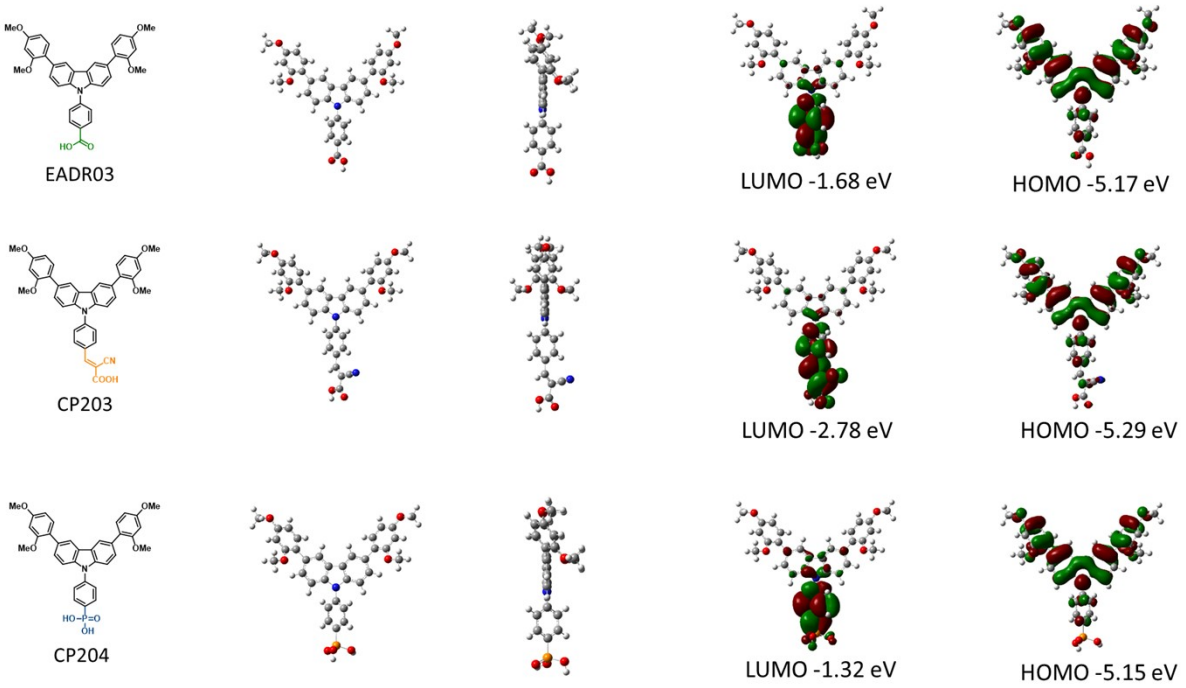

Fig. S14. The molecular structures and the calculated HOMO/LUMO orbitals and energy levels of EADR03, CP203 and CP204.

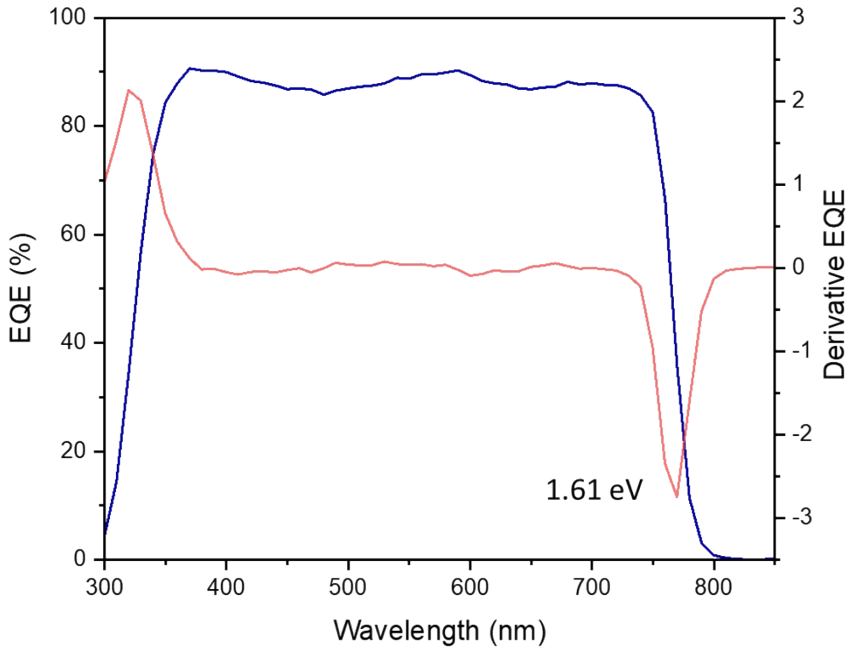

Fig. S15. External quantum efficiency (EQE) curve of the best **CP204** solar cell and the bandgap of perovskite ($Cs_{0.05}(FA_{0.85}MA_{0.15})_{0.95}Pb(I_{0.85}Br_{0.15})_3$) calculated from the derivative EQE spectrum. The integrated J_{SC} is 21.6 mA/cm^2, corresponding to the bandgap of 1.61 eV.

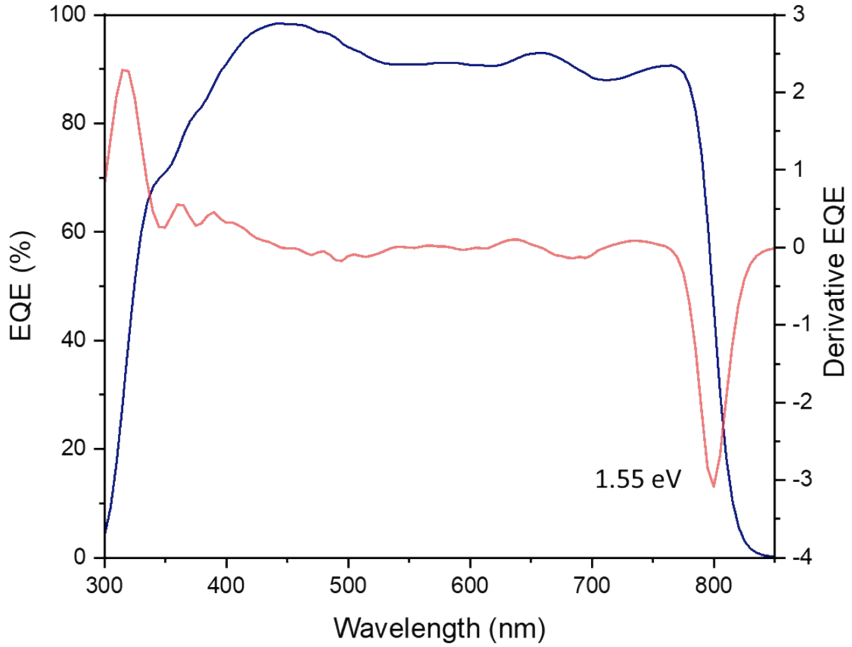

Fig. S16. EQE curve of the best **CP204** solar cell and the bandgap of perovskite ($Cs_{0.05}(FA_{0.99}MA_{0.01})_{0.95}Pb(I_{0.99}Br_{0.01})_3$) calculated from the derivative EQE spectrum. The integrated J_{SC} is 24.9 mA/cm^2, corresponding to the bandgap of 1.55 eV.

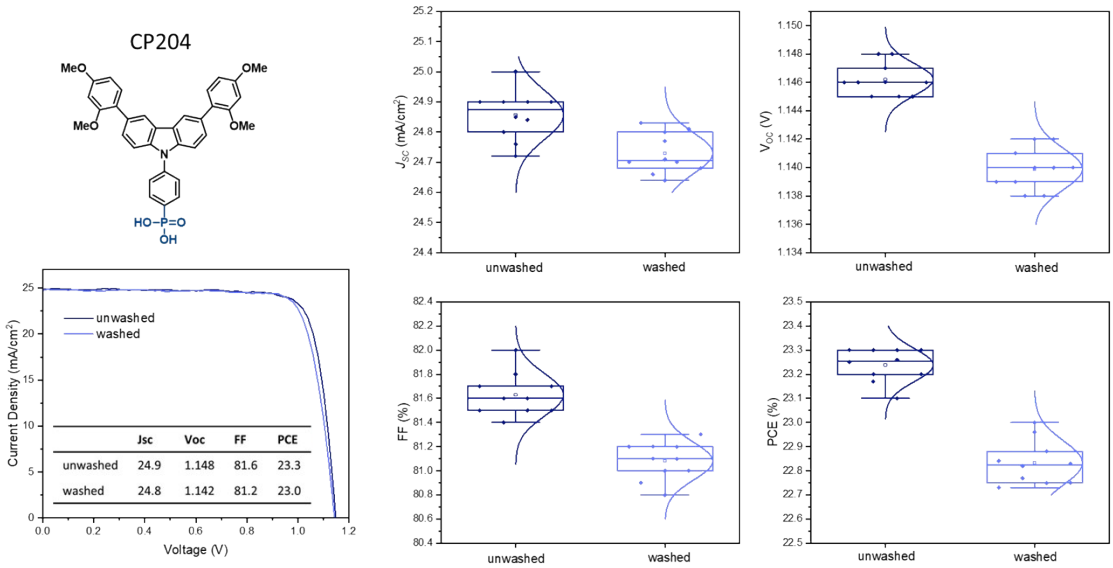

Fig. S17. Device performance with and without washing **CP204** after depositing SAM layer. The comparison is under the same batch.

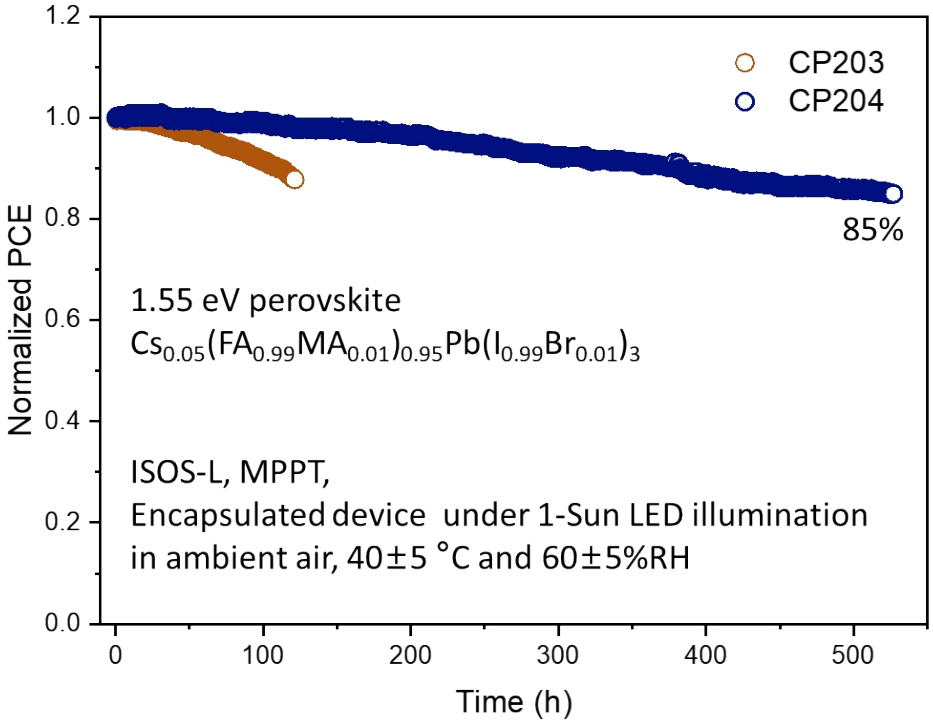

Fig. S18. The maximum power point tracking of CP203 and CP204 devices with 1.55 eV perovskite, using LED illumination under 1 sun of encapsulated solar cells in the ambient air (40±5 °C and 60±5% RH) under ISOS-L protocol.

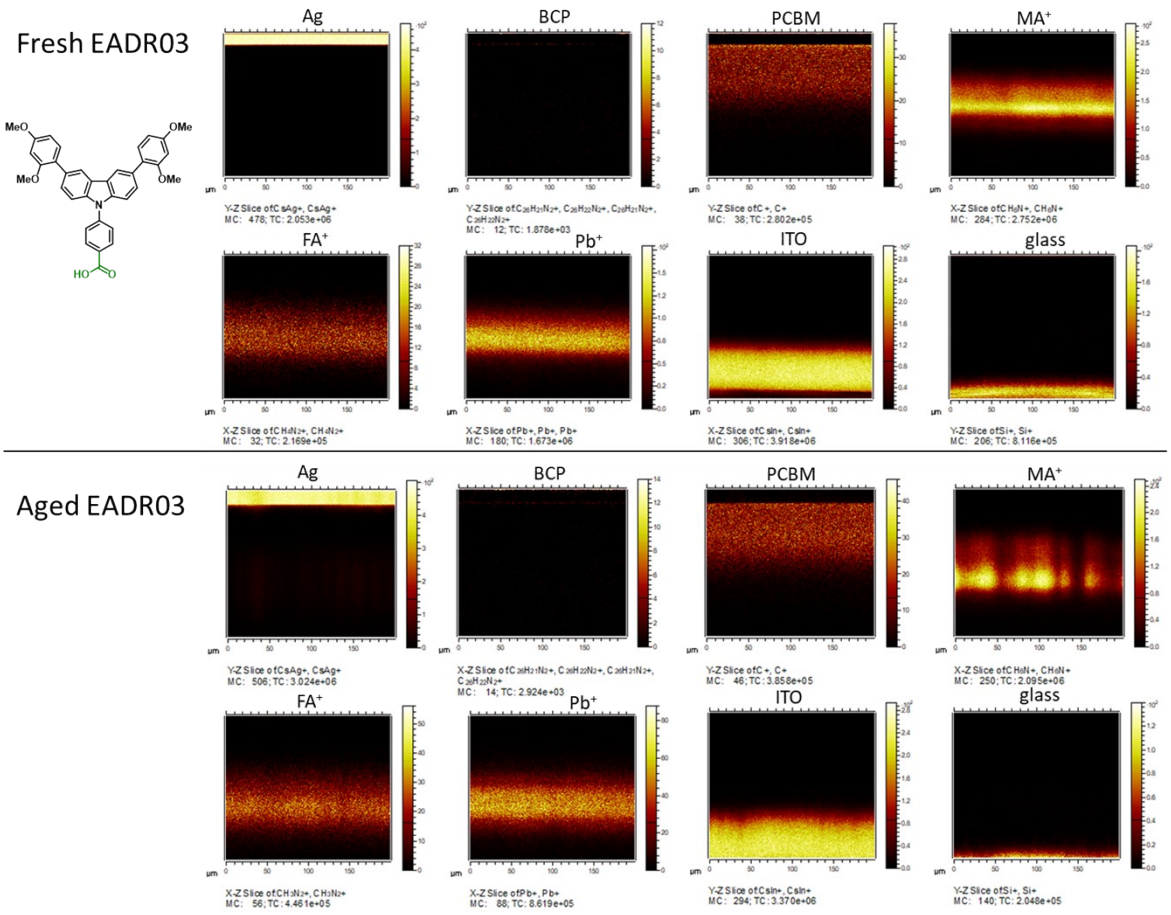

Fig. S19. The cross-section of ion distribution on fresh and aged devices with EADR03 SAM.

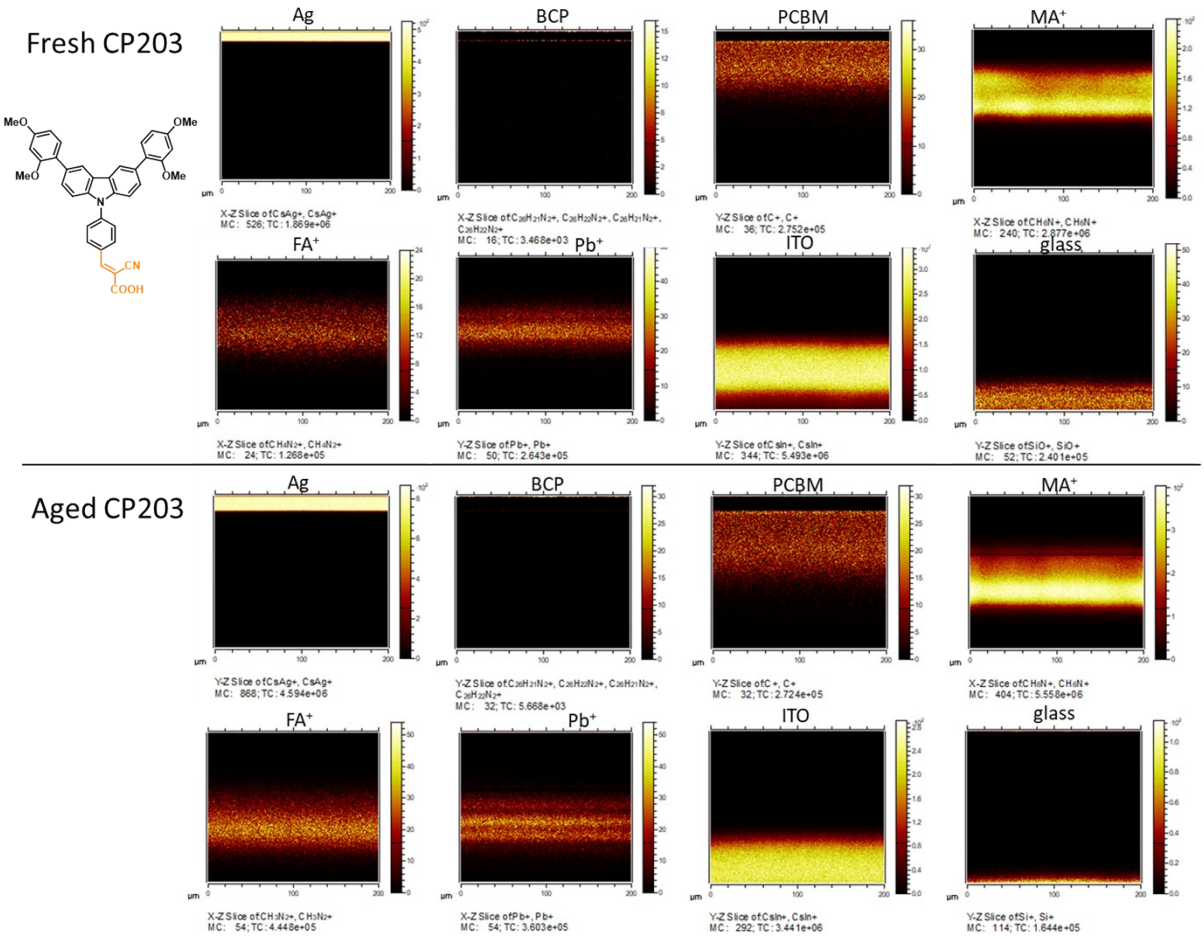

Fig. S20. The cross-section of ion distribution on fresh and aged devices with CP203 SAM.

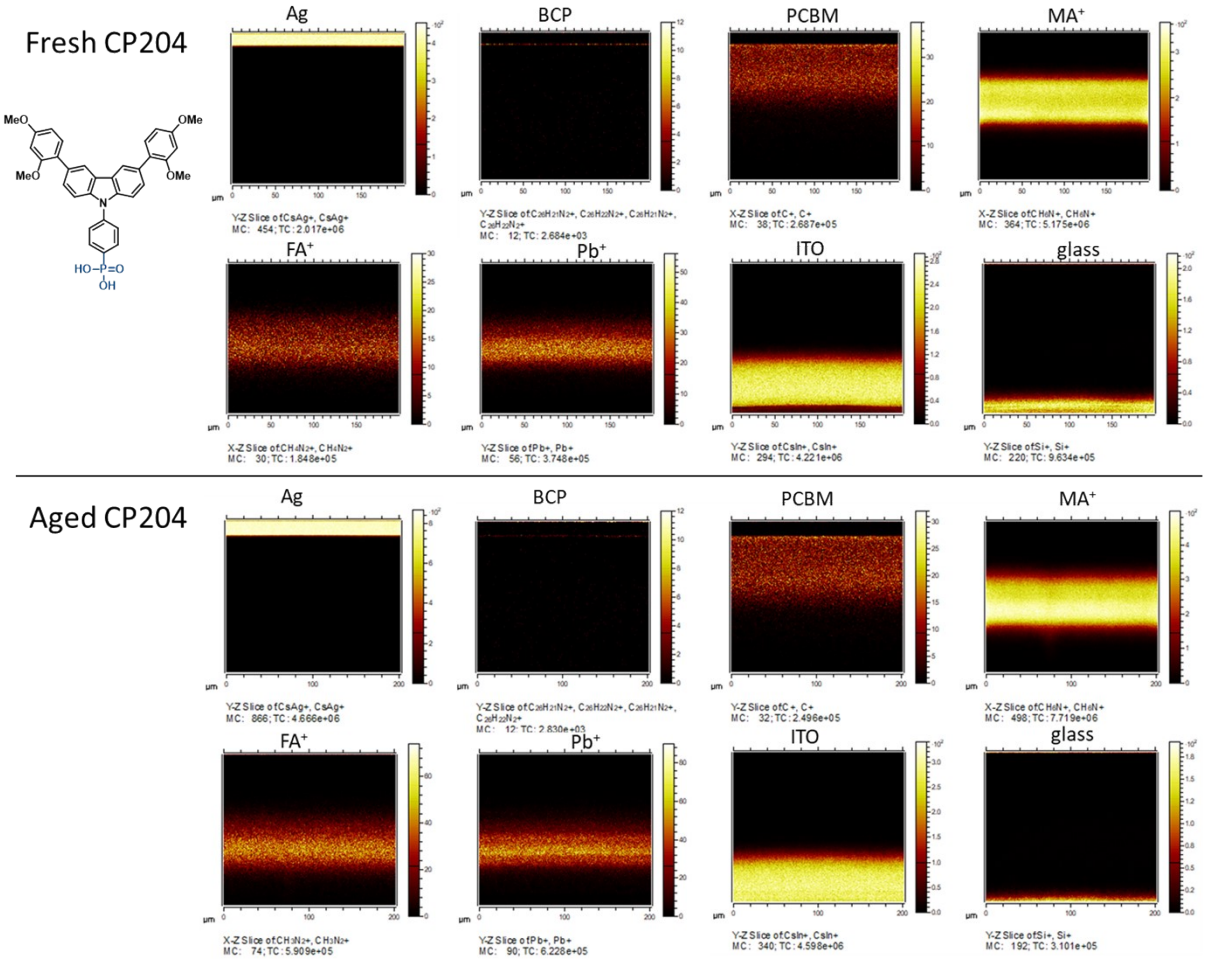

Fig. S21. The cross-section of ion distribution on fresh and aged devices with CP204 SAM.

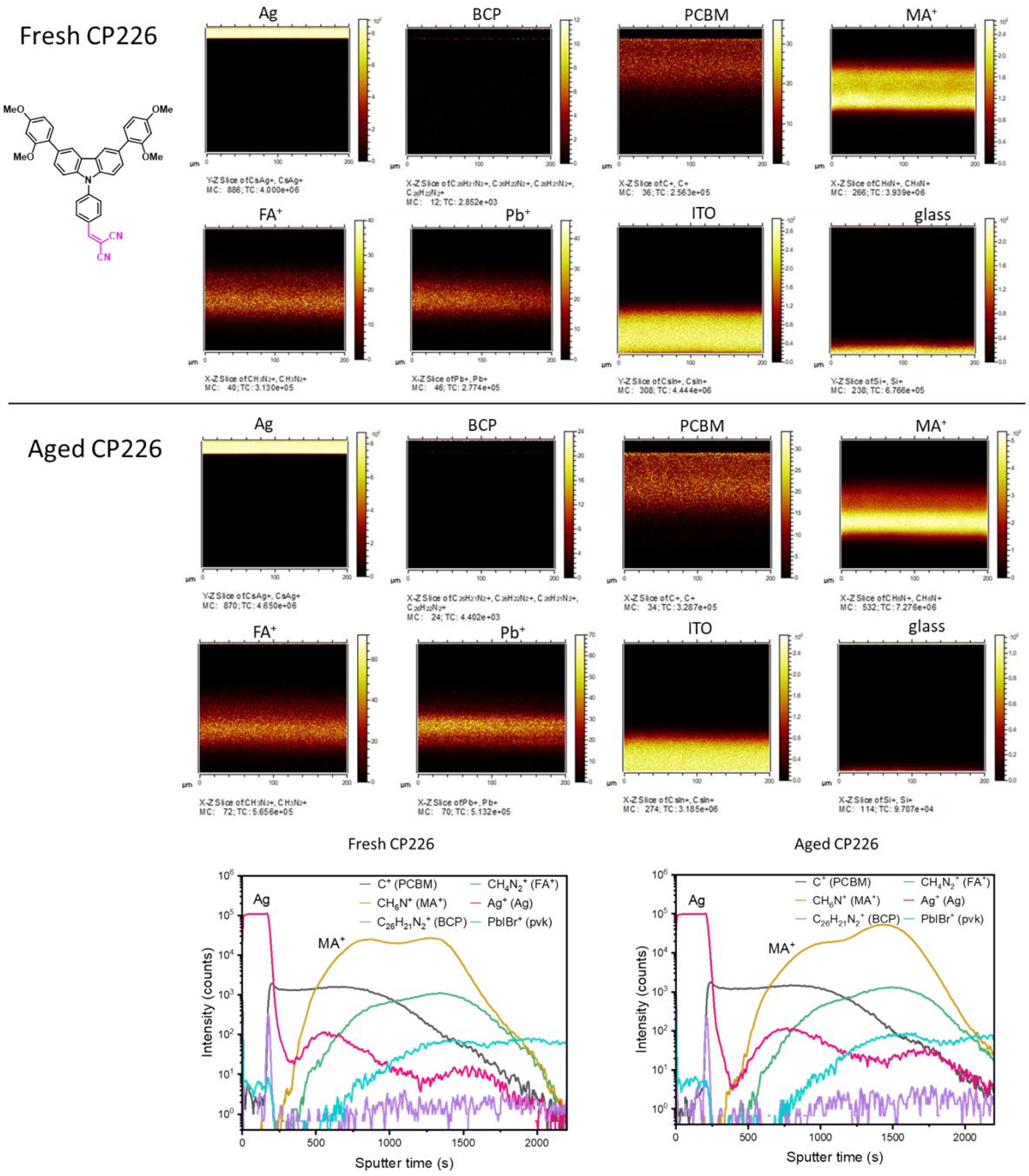

Fig. S22. The cross-section of ion distribution on fresh and aged devices with CP226 SAM.

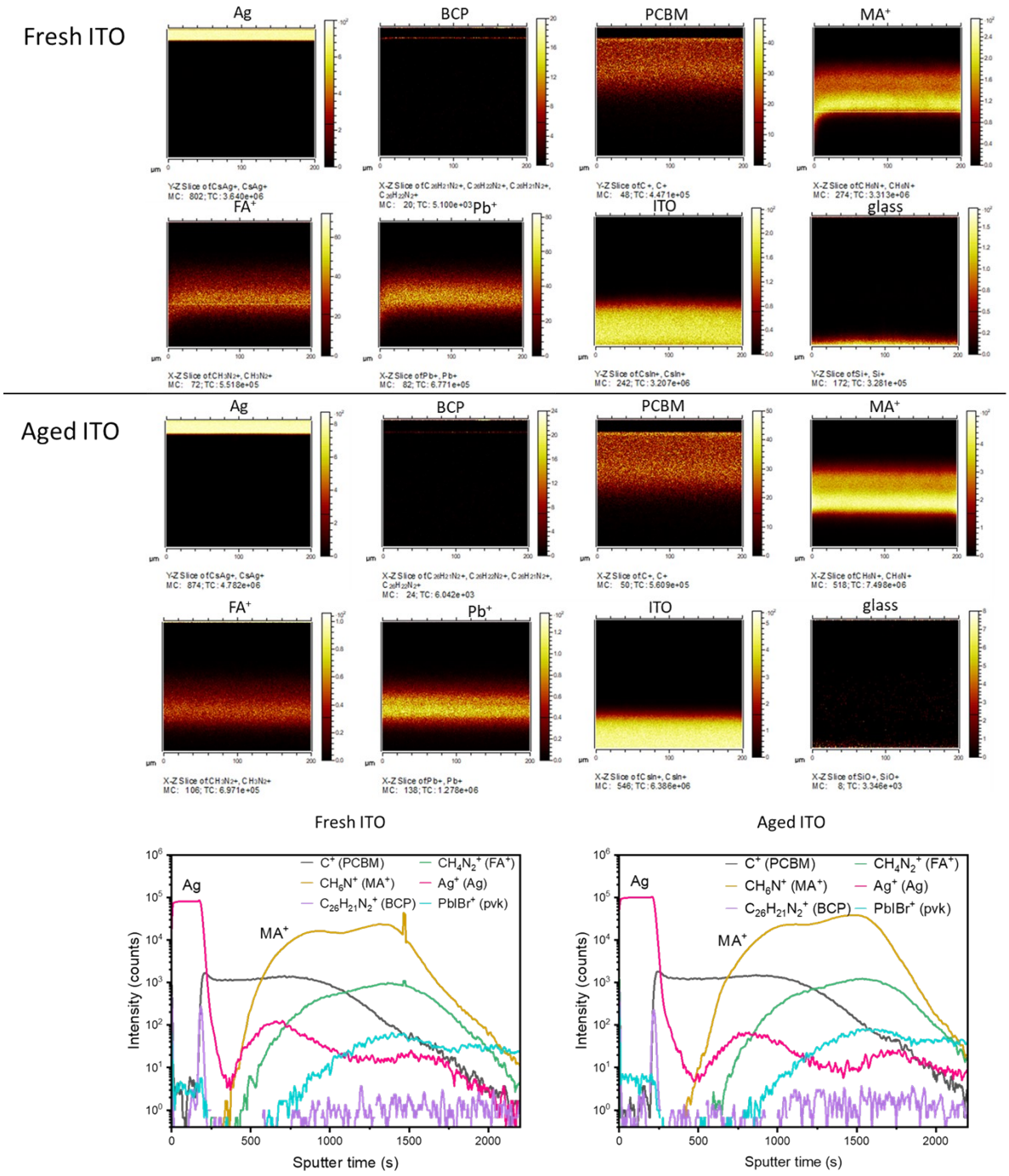

Fig. S23. The cross-section of ion distribution on fresh and aged devices with bare ITO.

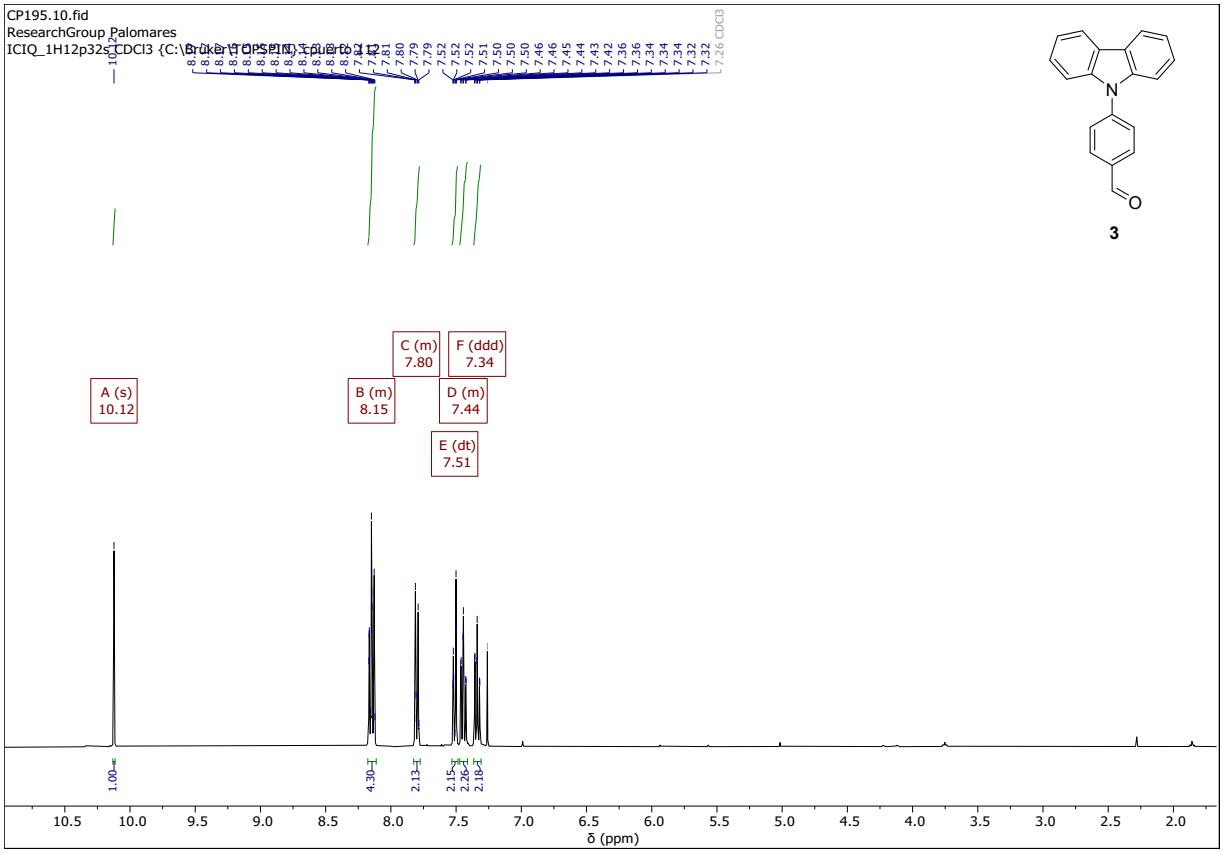

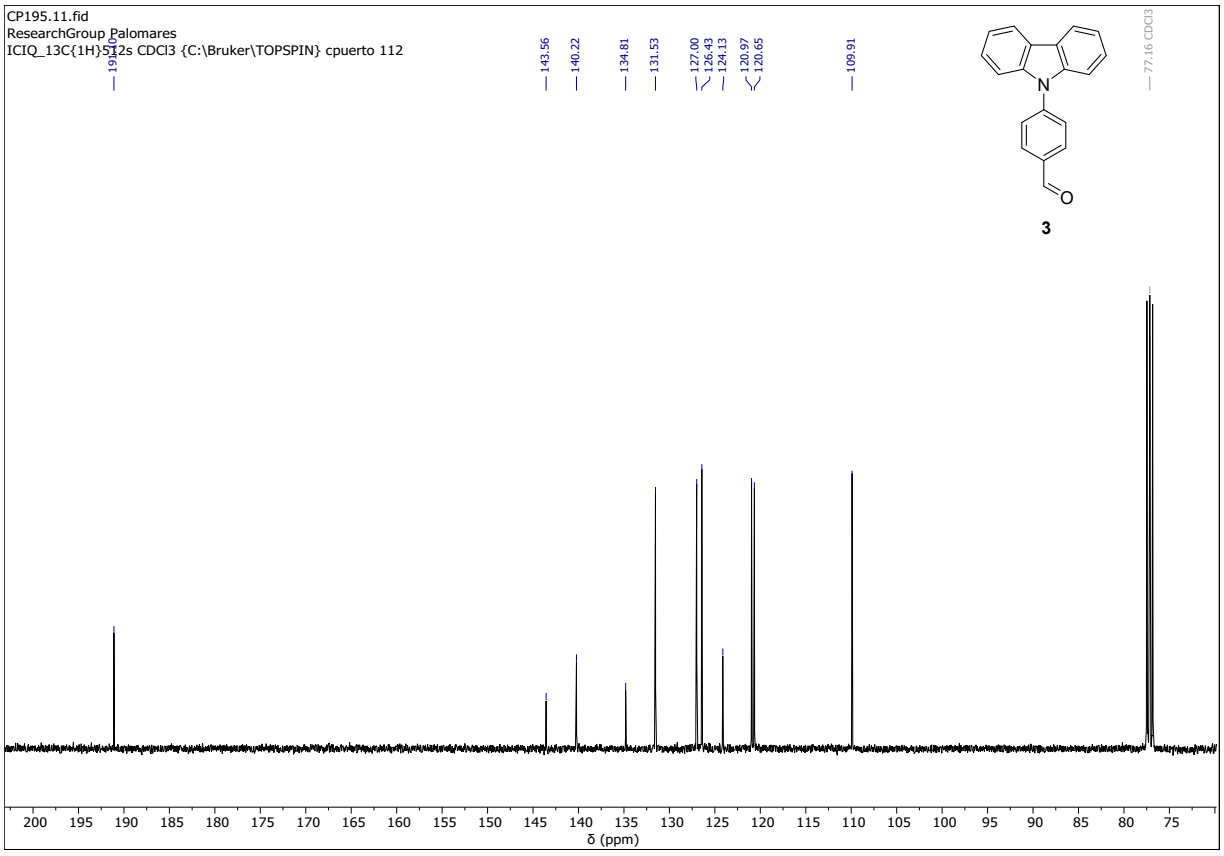

Fig. S24. ^{1}H NMR and ^{13}C NMR spectra for compound **3**.

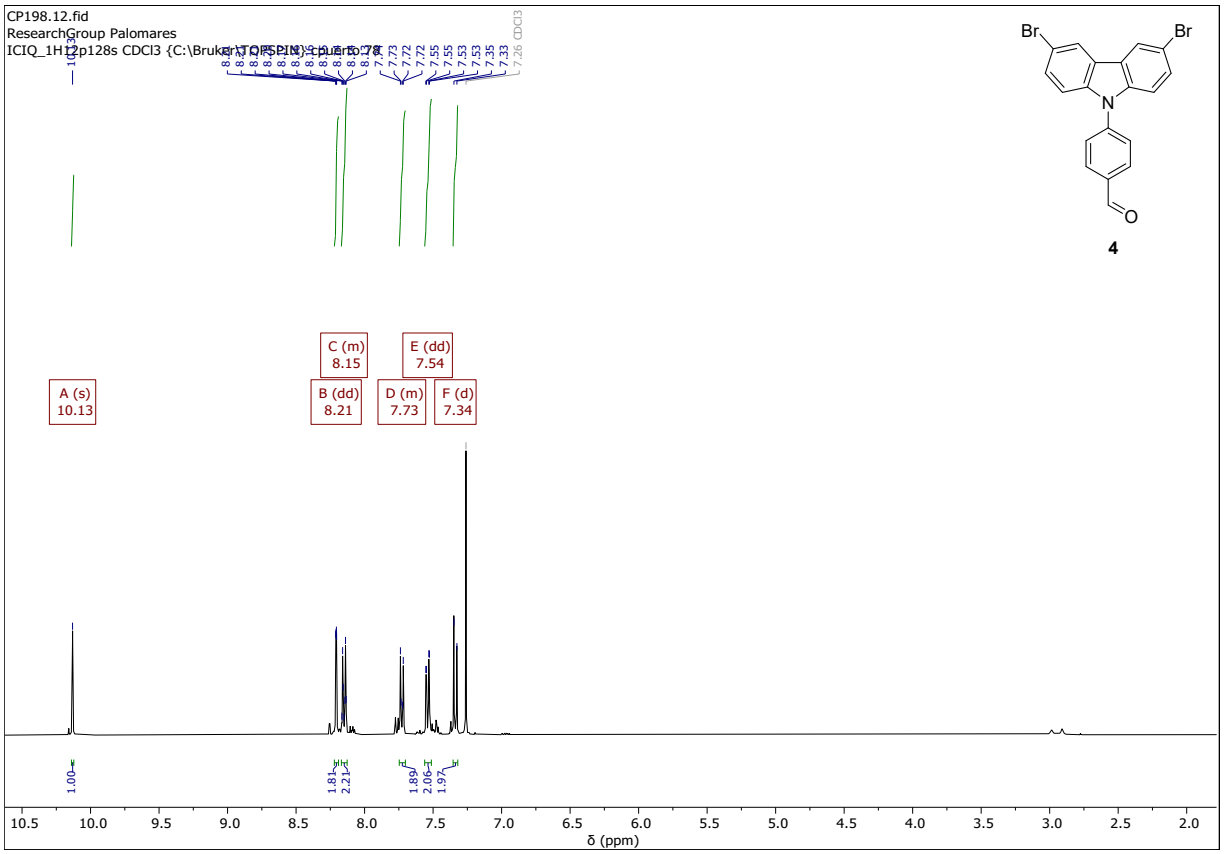
CP198.12.fid
ResearchGroup Palomares
ICIQ_1H_zg30_p128s CDCl3 {C:\Bruker\TOPSPIN} cpuerto 78
Br
Br
N
O
4
A (s)
10.13
B (dd)
8.21
C (m)
8.15
D (m)
7.73
E (dd)
7.54
F (d)
7.34
δ (ppm)

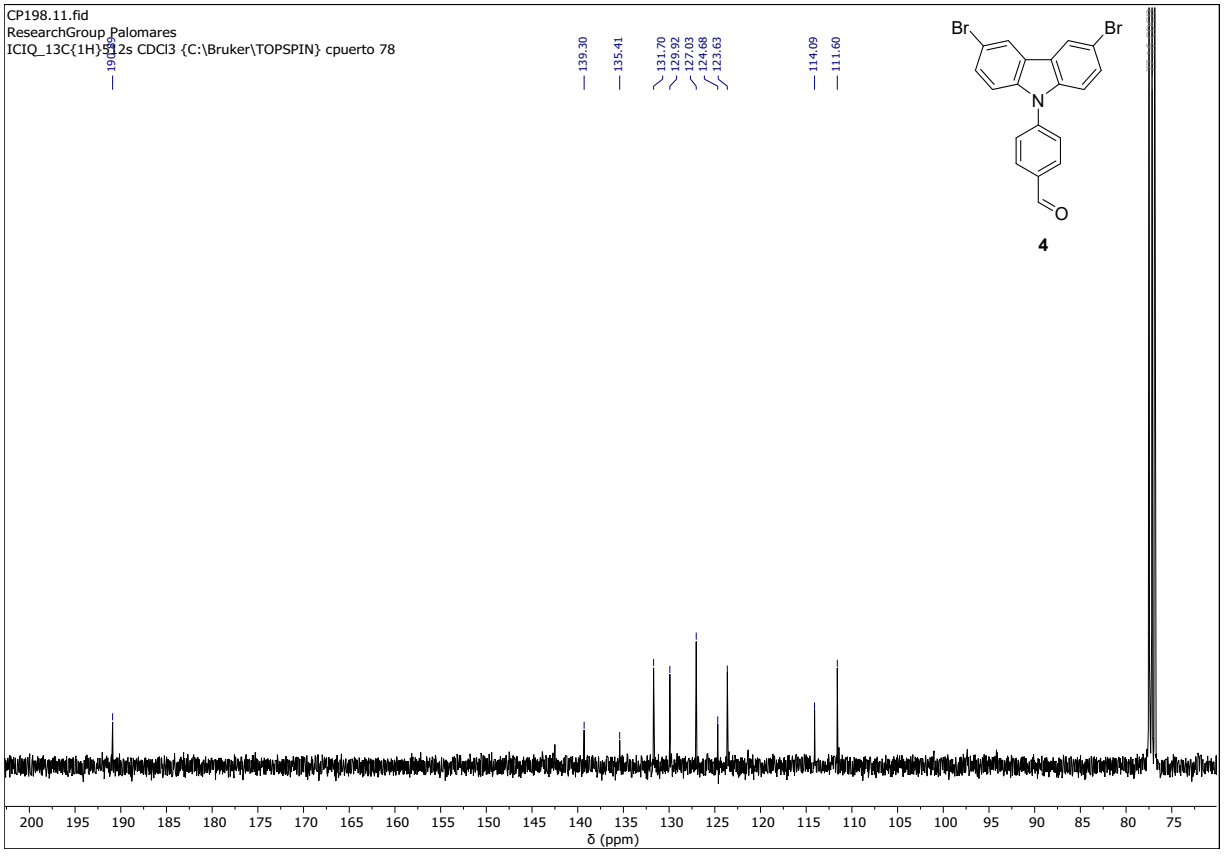
CP198.11.fid
ResearchGroup Palomares
ICIQ_13C{1H}_512s CDCl3 {C:\Bruker\TOPSPIN} cpuerto 78
139.30
135.41
131.70
129.92
127.03
124.68
123.63
114.09
111.60
Br
Br
N
O
4
δ (ppm)

Fig. S25. ^{1}H NMR and ^{13}C NMR spectra for compound **4**.

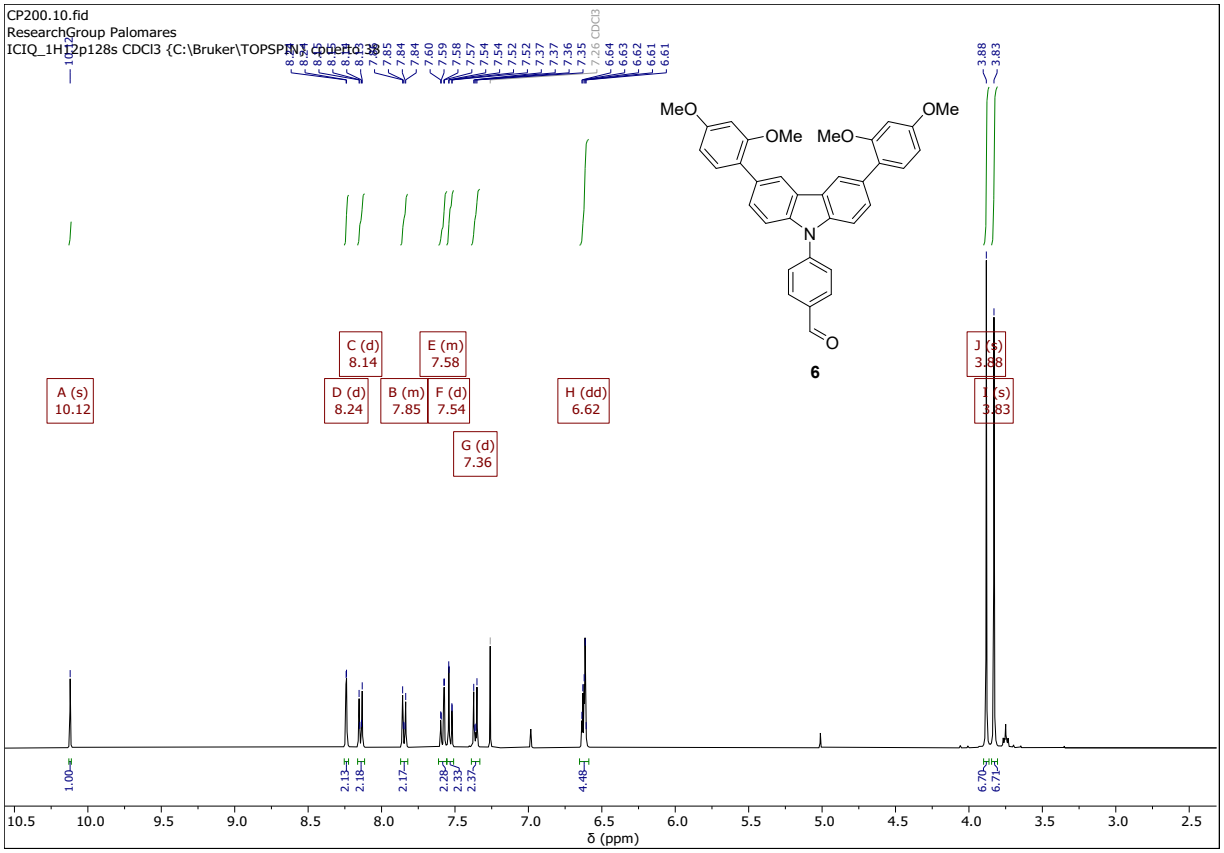

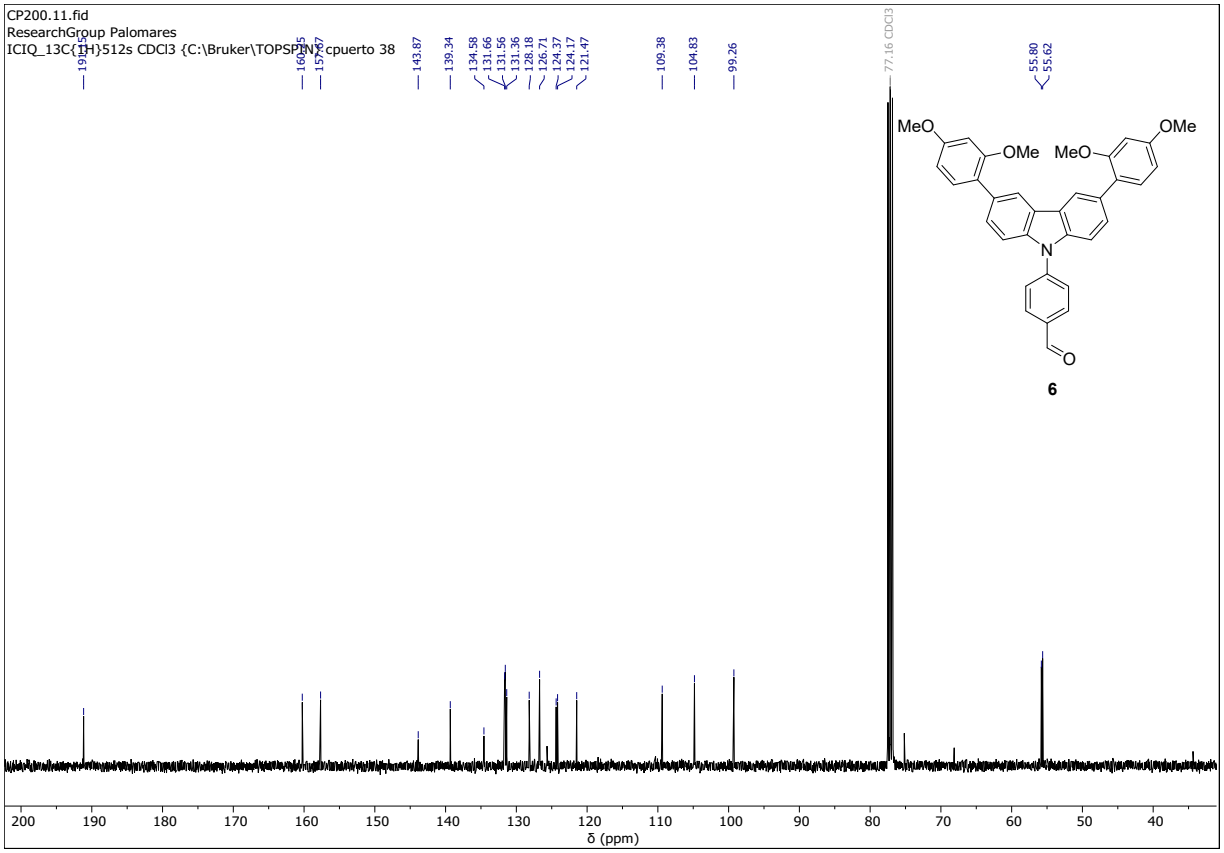

Fig. S26. ^{1}H NMR and ^{13}C NMR spectra for compound **6**.

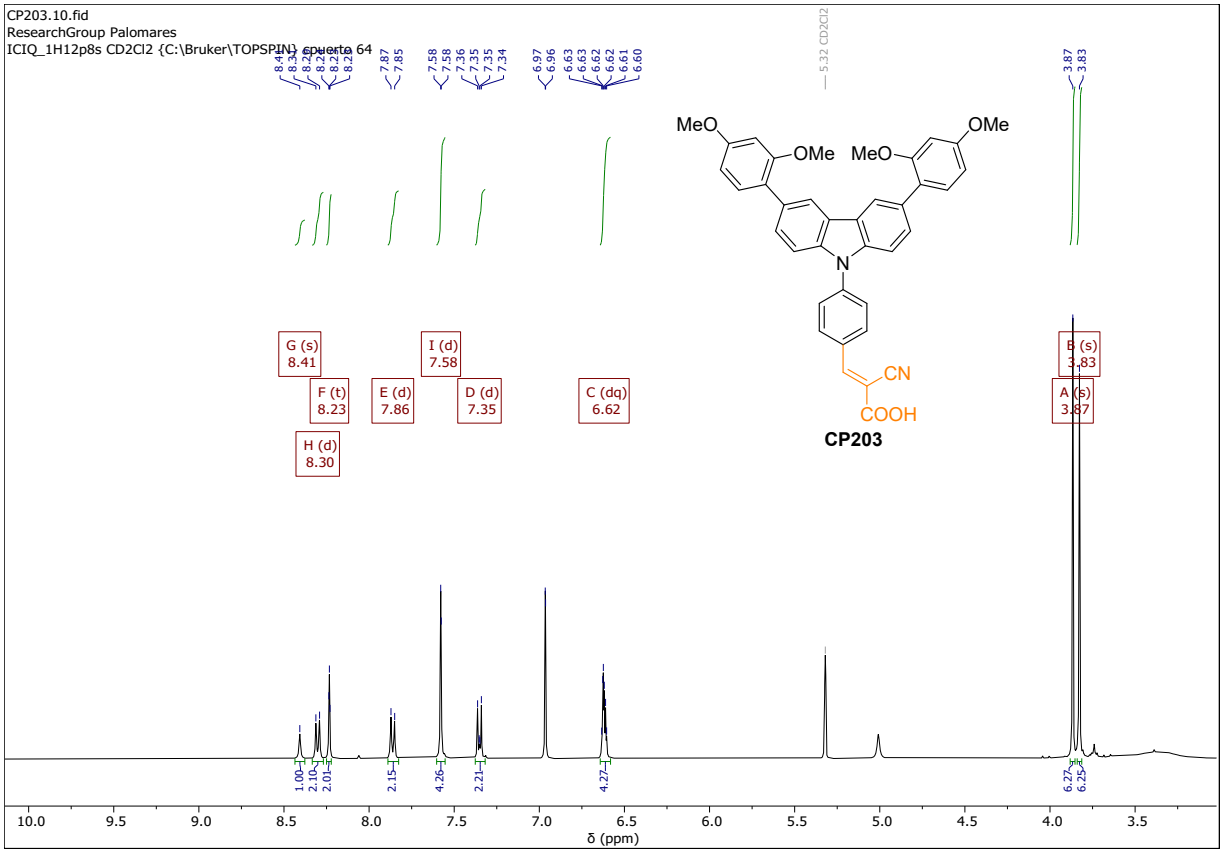

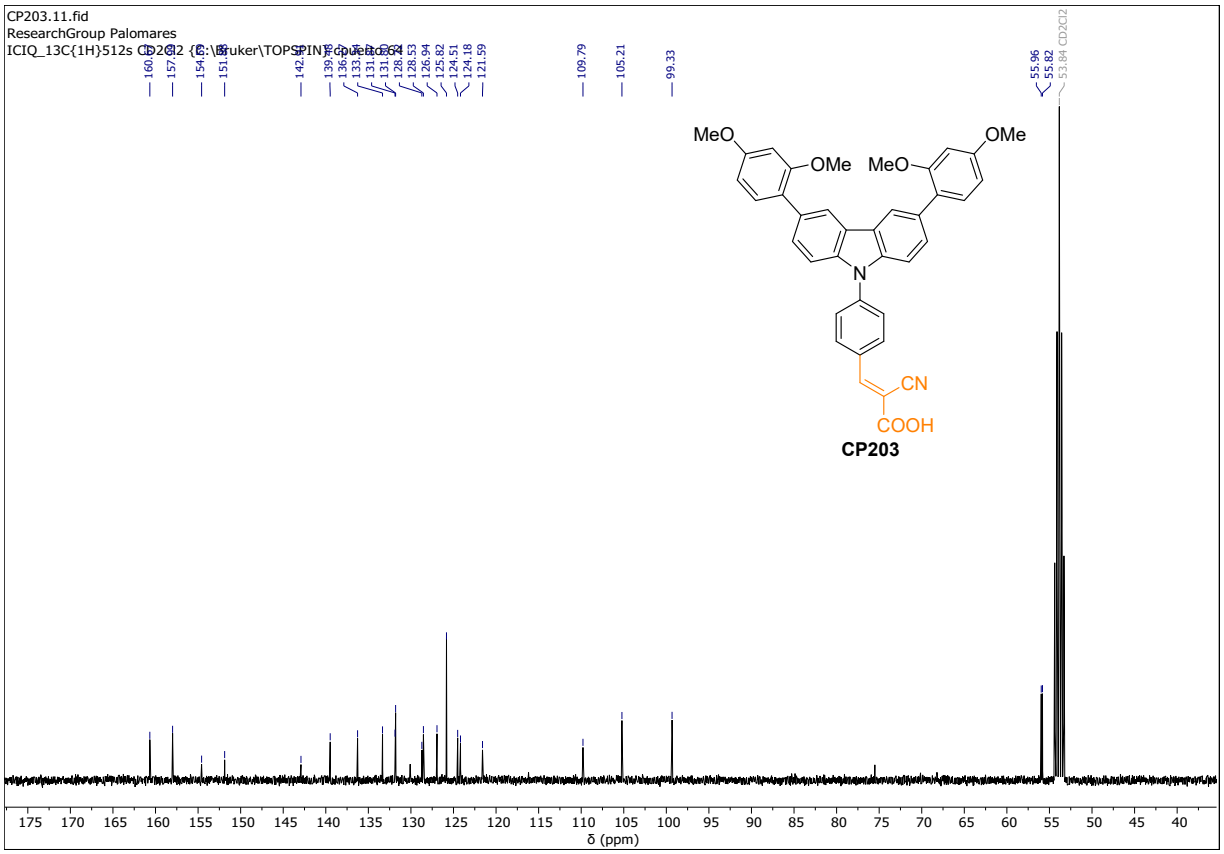

Fig. S27. ^{1}H NMR and ^{13}C NMR spectra for SAM **CP203**.

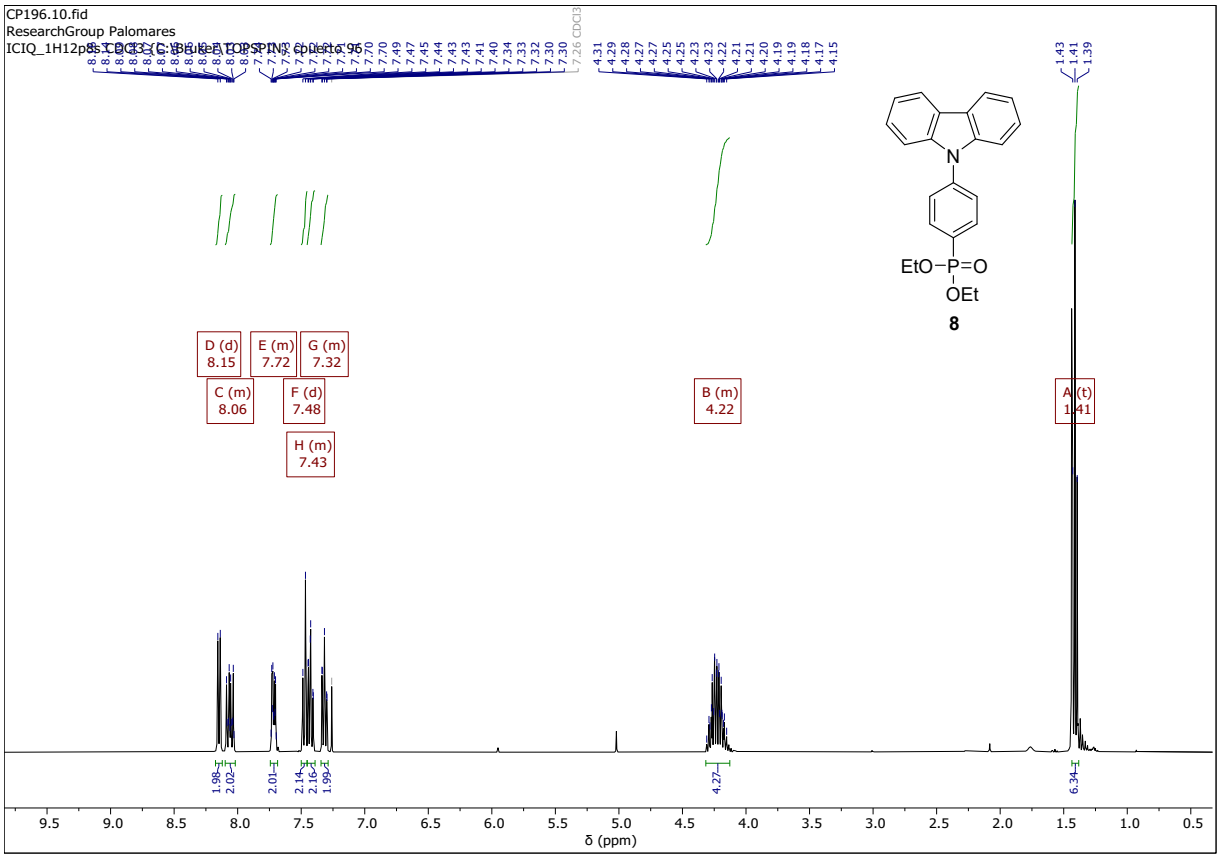
CP196.10.fid
ResearchGroup Palomares
D (d) 8.15
E (m) 7.72
G (m) 7.32
C (m) 8.06
F (d) 7.48
H (m) 7.43
B (m) 4.22
A (t) 1.41
EtO−P=O
OEt
8
δ (ppm)

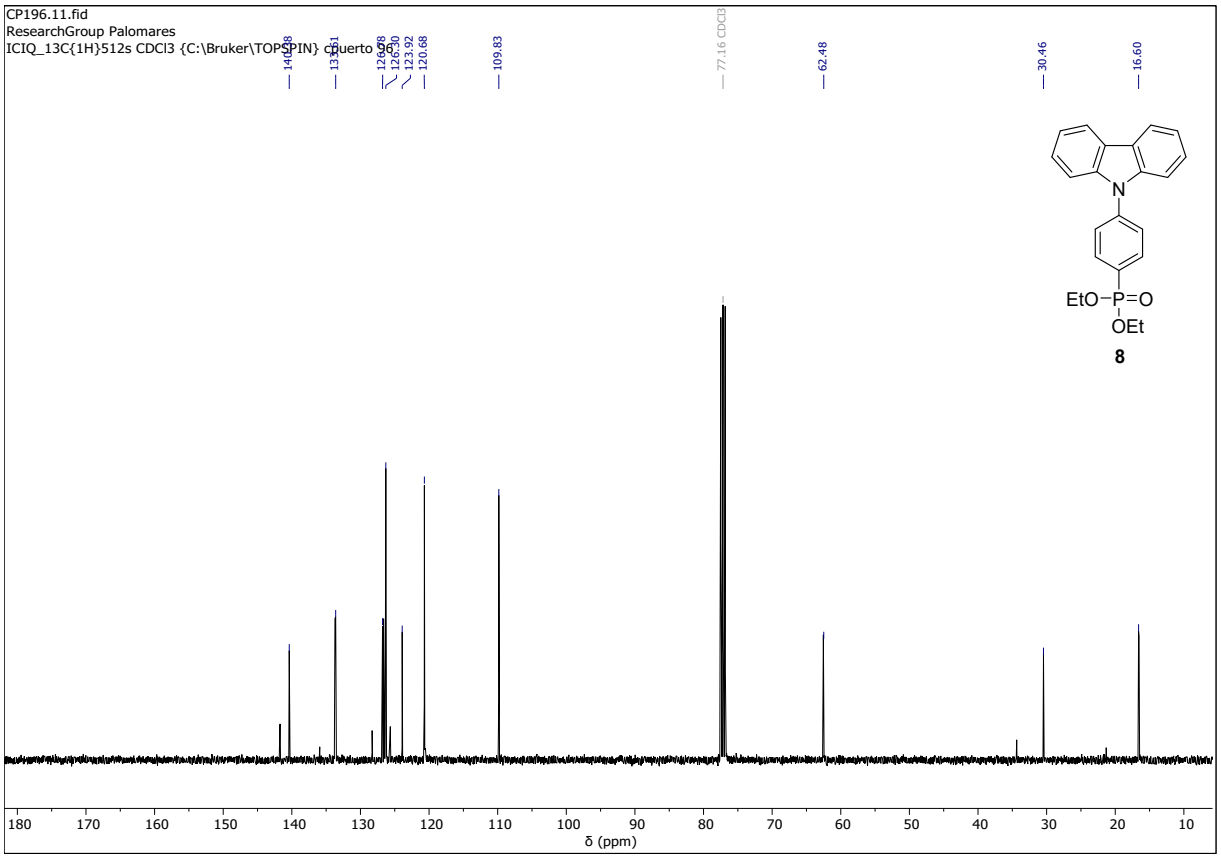
CP196.11.fid
ResearchGroup Palomares
140.88
133.01
126.98
126.80
123.92
120.68
109.83
77.16 CDCl3
62.48
30.46
16.60
EtO−P=O
OEt
8
δ (ppm)

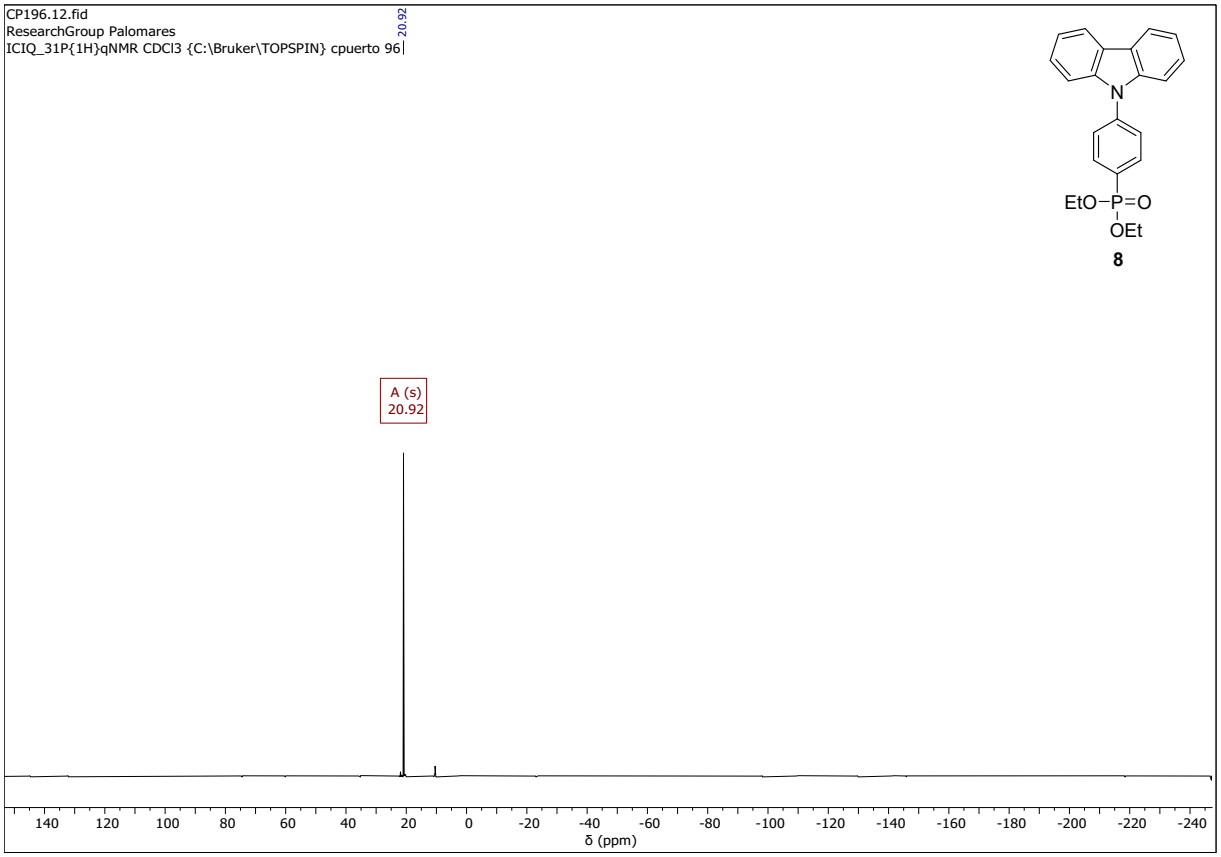

Fig. S28. ^{1}H NMR, ^{13}C NMR and ^{31}P NMR spectra for compound **8**.

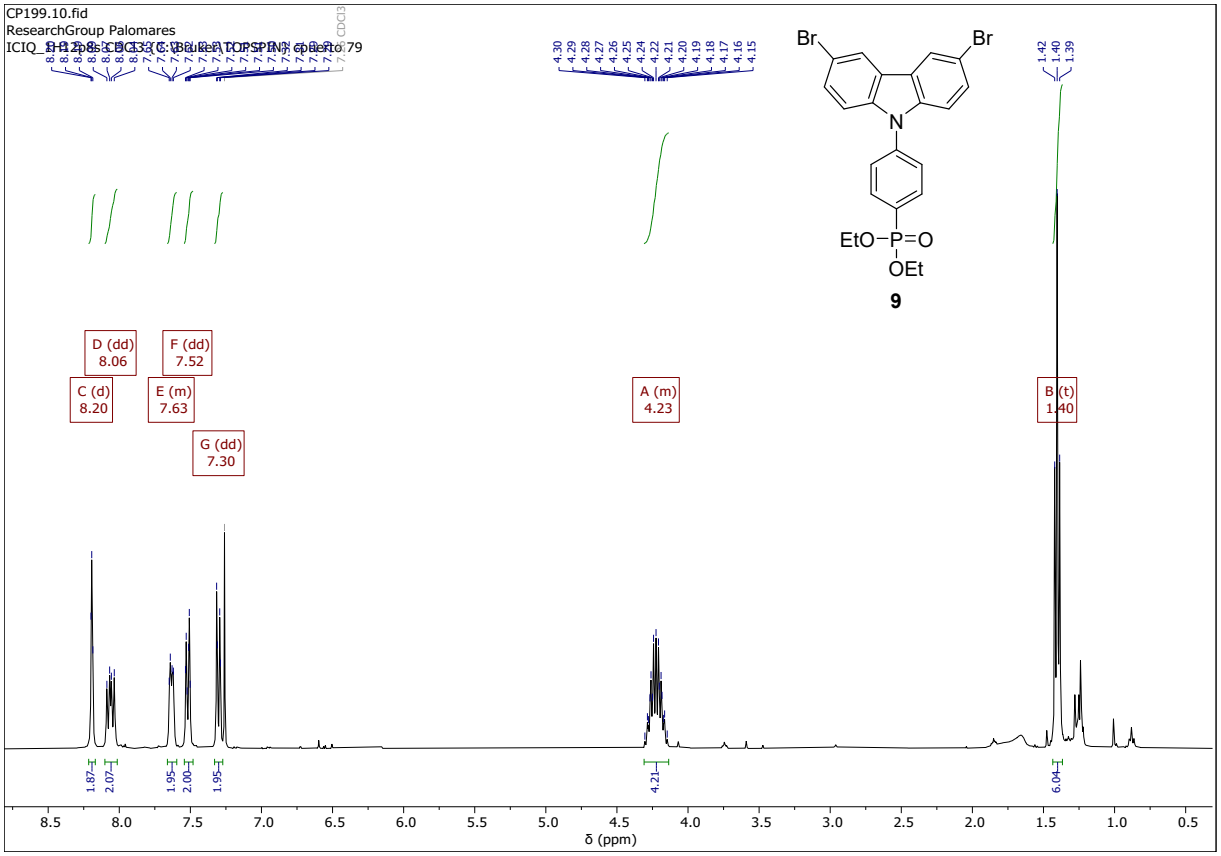
CP199.10.fid
ResearchGroup Palomares
Br
Br
N
EtO−P=O
OEt
9
D (dd) 8.06
F (dd) 7.52
C (d) 8.20
E (m) 7.63
G (dd) 7.30
A (m) 4.23
B (t) 1.40
δ (ppm)

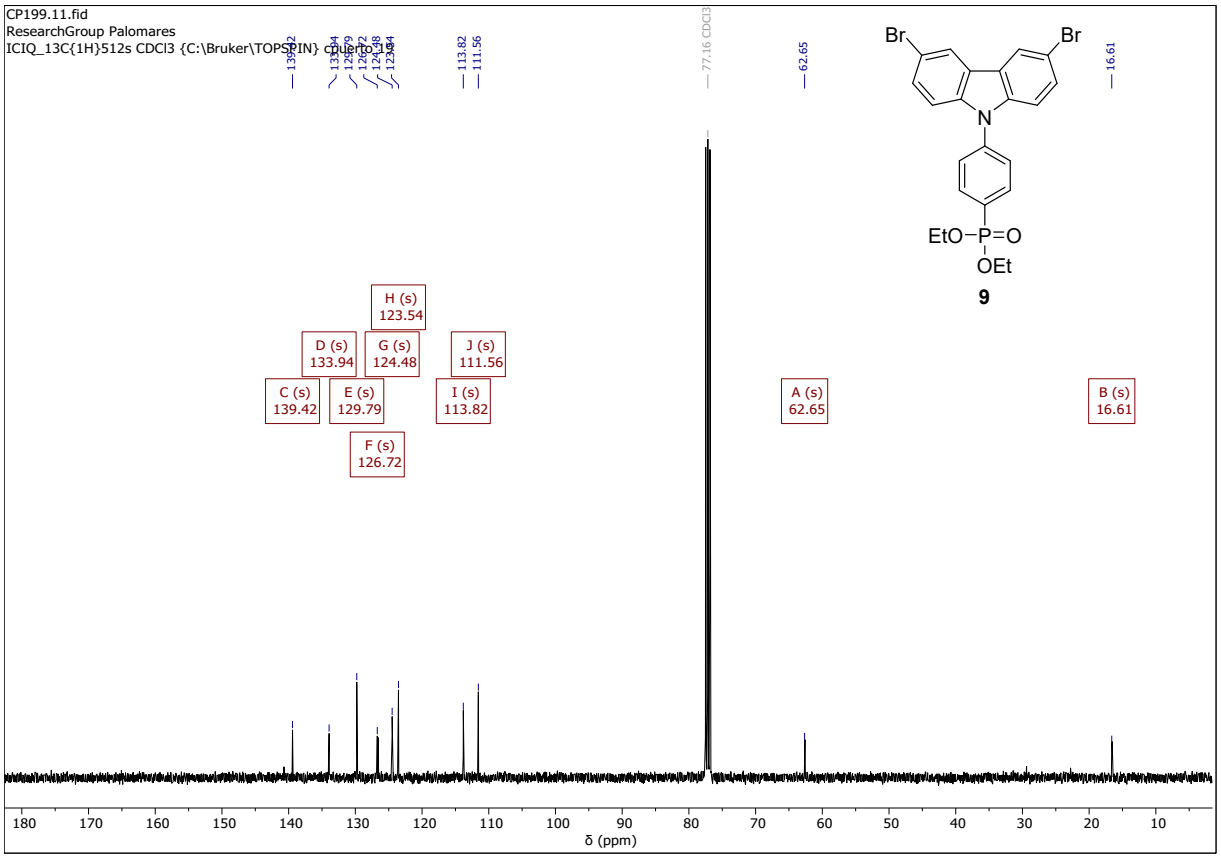
CP199.11.fid
ResearchGroup Palomares
Br
Br
N
EtO−P=O
OEt
9
H (s) 123.54
D (s) 133.94
G (s) 124.48
J (s) 111.56
C (s) 139.42
E (s) 129.79
I (s) 113.82
A (s) 62.65
B (s) 16.61
F (s) 126.72
δ (ppm)

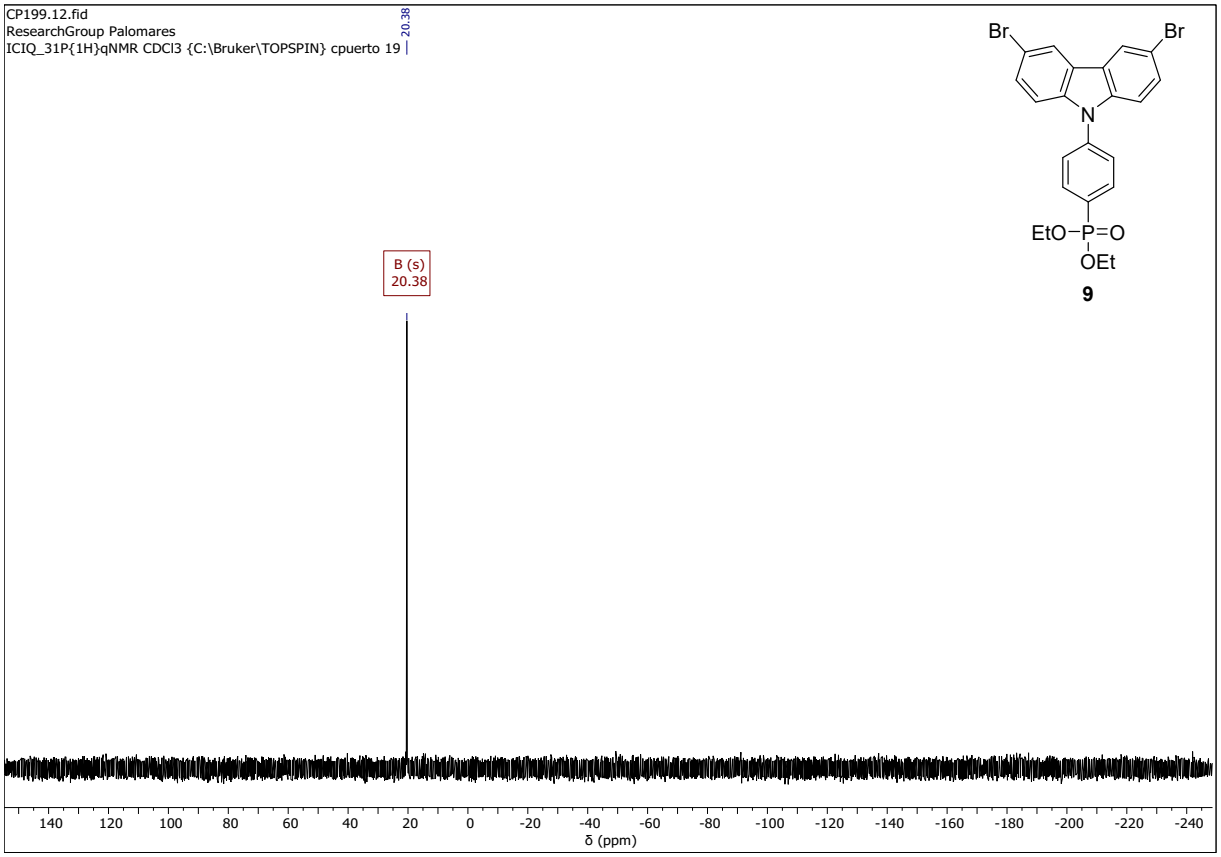

Fig. S29. ^{1}H NMR, ^{13}C NMR and ^{31}P NMR spectra for compound **9**.

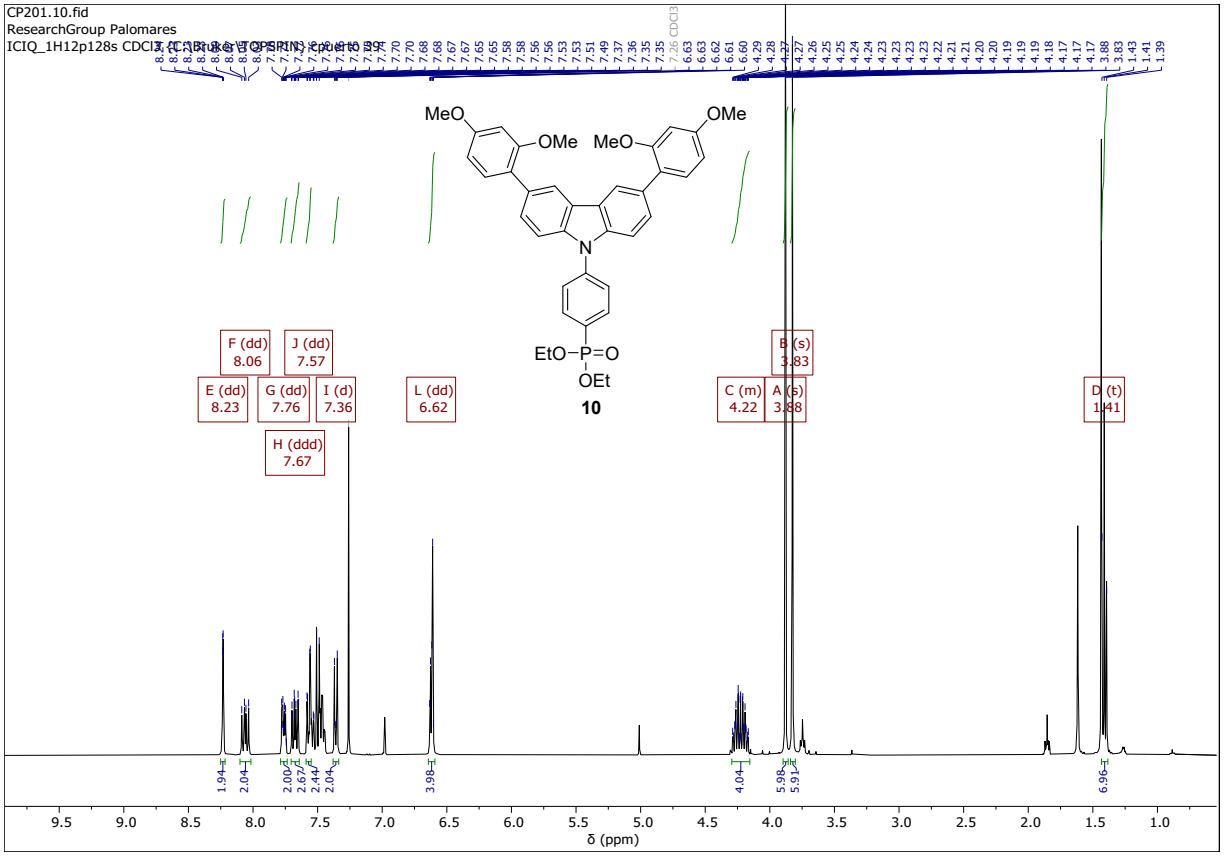
CP201.10.fid
ResearchGroup Palomares
ICIQ_1H12p128s CDCl3 {C:\Bruker\TOPSPIN} cpdprg1 39
MeO
OMe
MeO
OMe
N
EtO−P=O
OEt
10
F (dd) 8.06
J (dd) 7.57
E (dd) 8.23
G (dd) 7.76
I (d) 7.36
H (ddd) 7.67
L (dd) 6.62
B (s) 3.83
C (m) 4.22
A (s) 3.88
D (t) 1.41
δ (ppm)

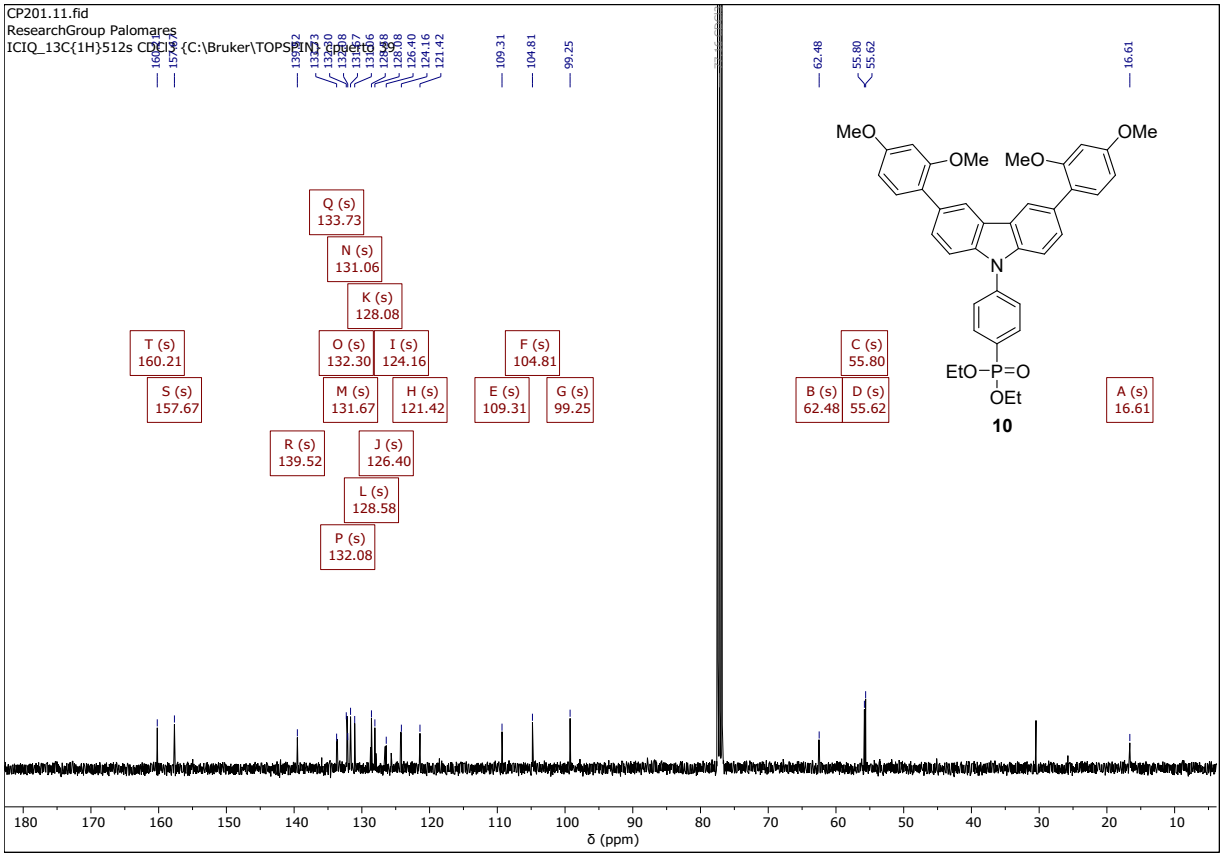
CP201.11.fid
ResearchGroup Palomares
ICIQ_13C{1H}512s CDCl3 {C:\Bruker\TOPSPIN} cpdprg1 39
MeO
OMe
MeO
OMe
N
EtO−P=O
OEt
10
Q (s) 133.73
N (s) 131.06
K (s) 128.08
T (s) 160.21
O (s) 132.30
I (s) 124.16
F (s) 104.81
S (s) 157.67
M (s) 131.67
H (s) 121.42
E (s) 109.31
G (s) 99.25
R (s) 139.52
J (s) 126.40
L (s) 128.58
P (s) 132.08
C (s) 55.80
B (s) 62.48
D (s) 55.62
A (s) 16.61
δ (ppm)

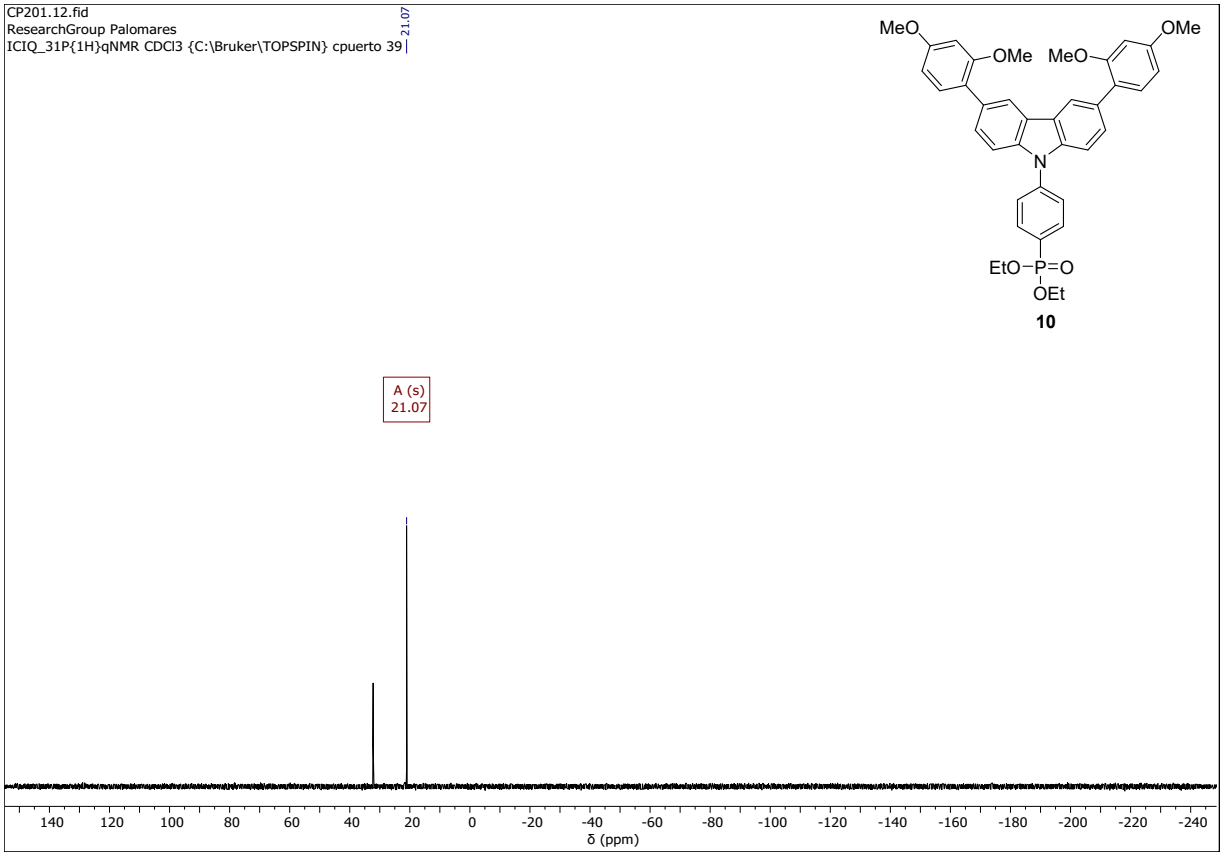

Fig. S30. ^{1}H NMR, ^{13}C NMR and ^{31}P NMR spectra for compound **10**.

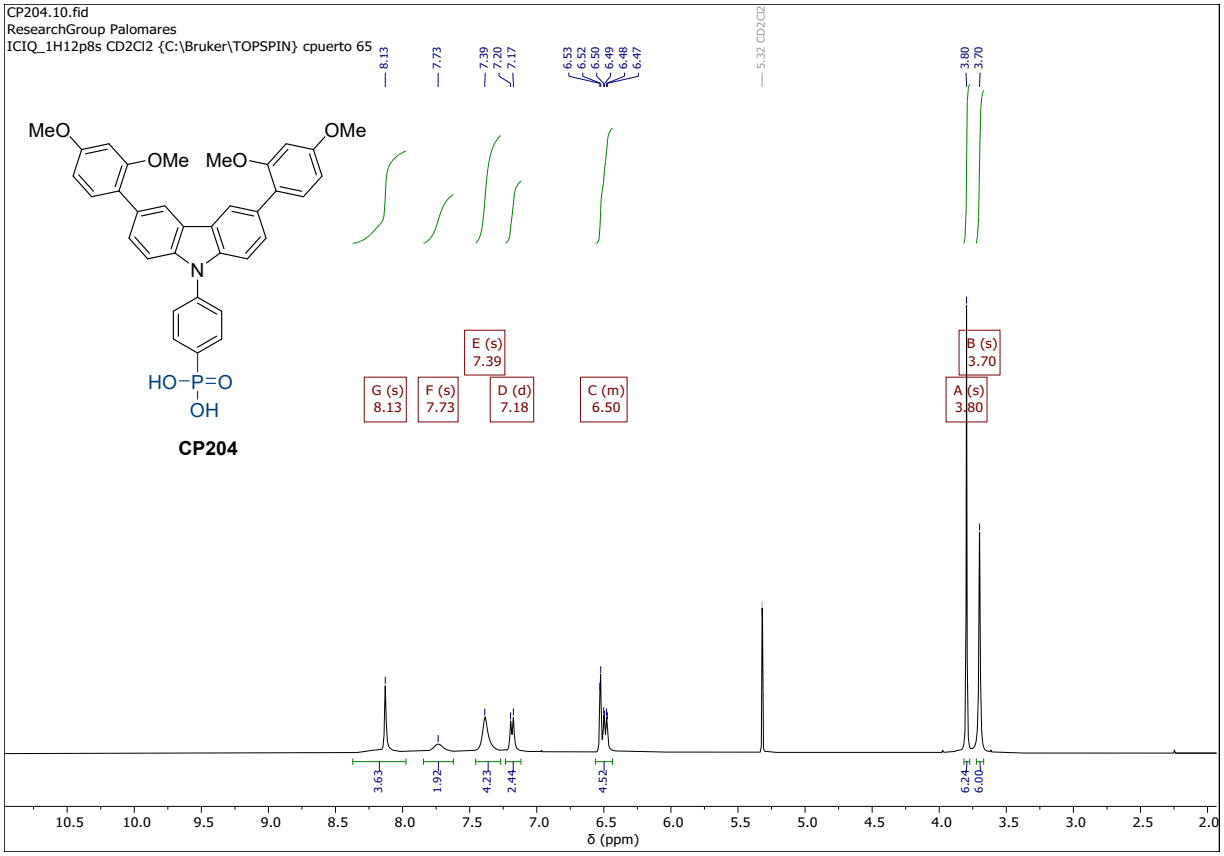
CP204.10.fid
ResearchGroup Palomares
ICIQ_1H12p8s CD2Cl2 {C:\Bruker\TOPSPIN} cpuerto 65
MeO
OMe
MeO
OMe
N
HO−P=O
OH
CP204
E (s) 7.39
G (s) 8.13
F (s) 7.73
D (d) 7.18
C (m) 6.50
B (s) 3.70
A (s) 3.80
δ (ppm)

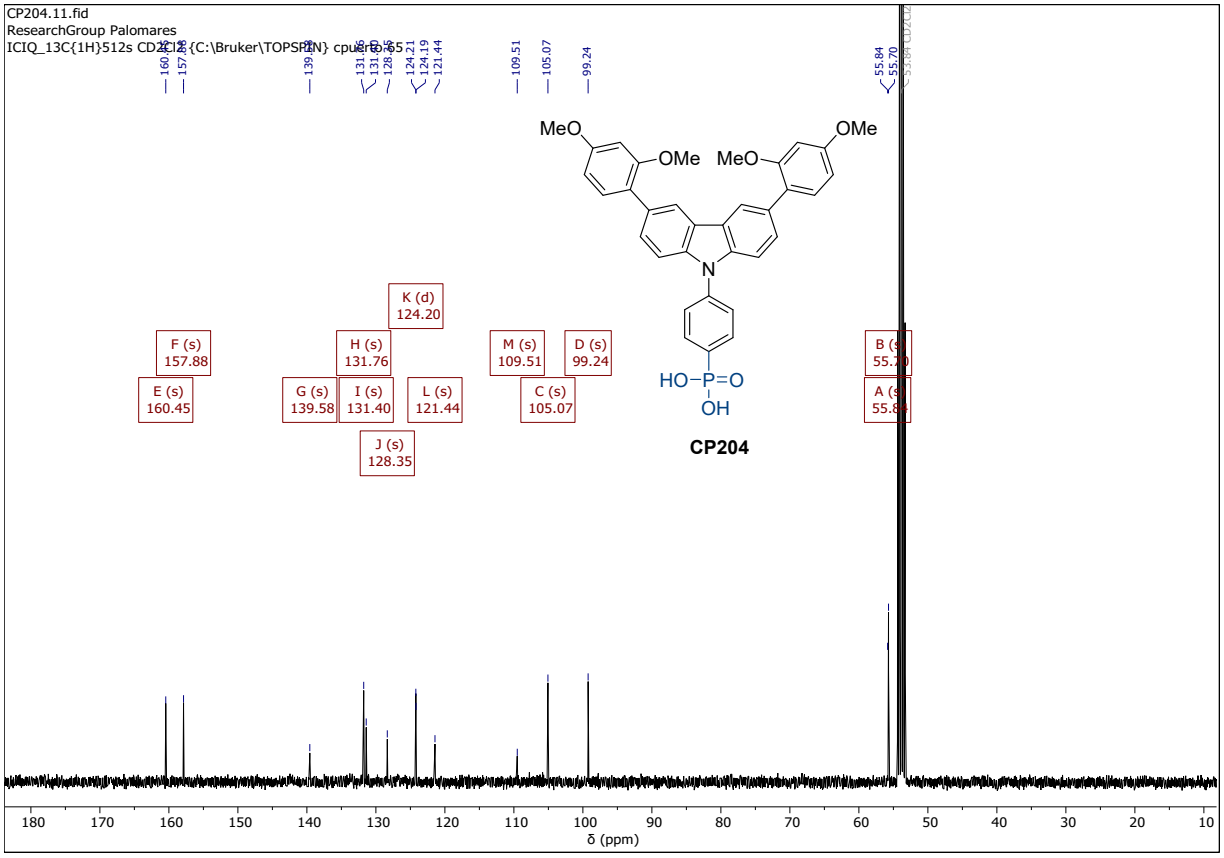
CP204.11.fid
ResearchGroup Palomares
ICIQ_13C{1H}512s CD2Cl2 {C:\Bruker\TOPSPIN} cpuerto 65
MeO
OMe
MeO
OMe
N
HO−P=O
OH
CP204
K (d) 124.20
F (s) 157.88
H (s) 131.76
M (s) 109.51
D (s) 99.24
E (s) 160.45
G (s) 139.58
I (s) 131.40
L (s) 121.44
C (s) 105.07
J (s) 128.35
δ (ppm)

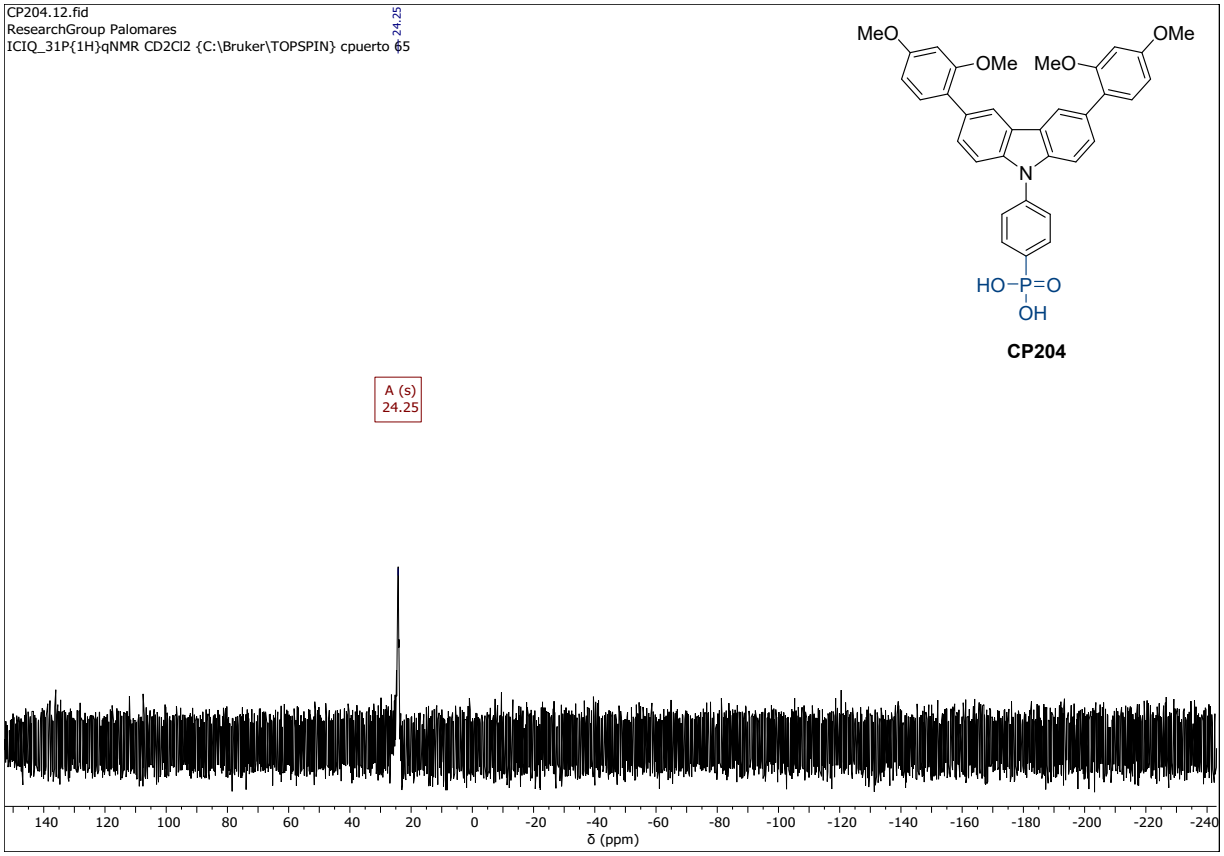

Fig. S31. ^{1}H NMR, ^{13}C NMR and ^{31}P NMR spectra for SAM **CP204**.

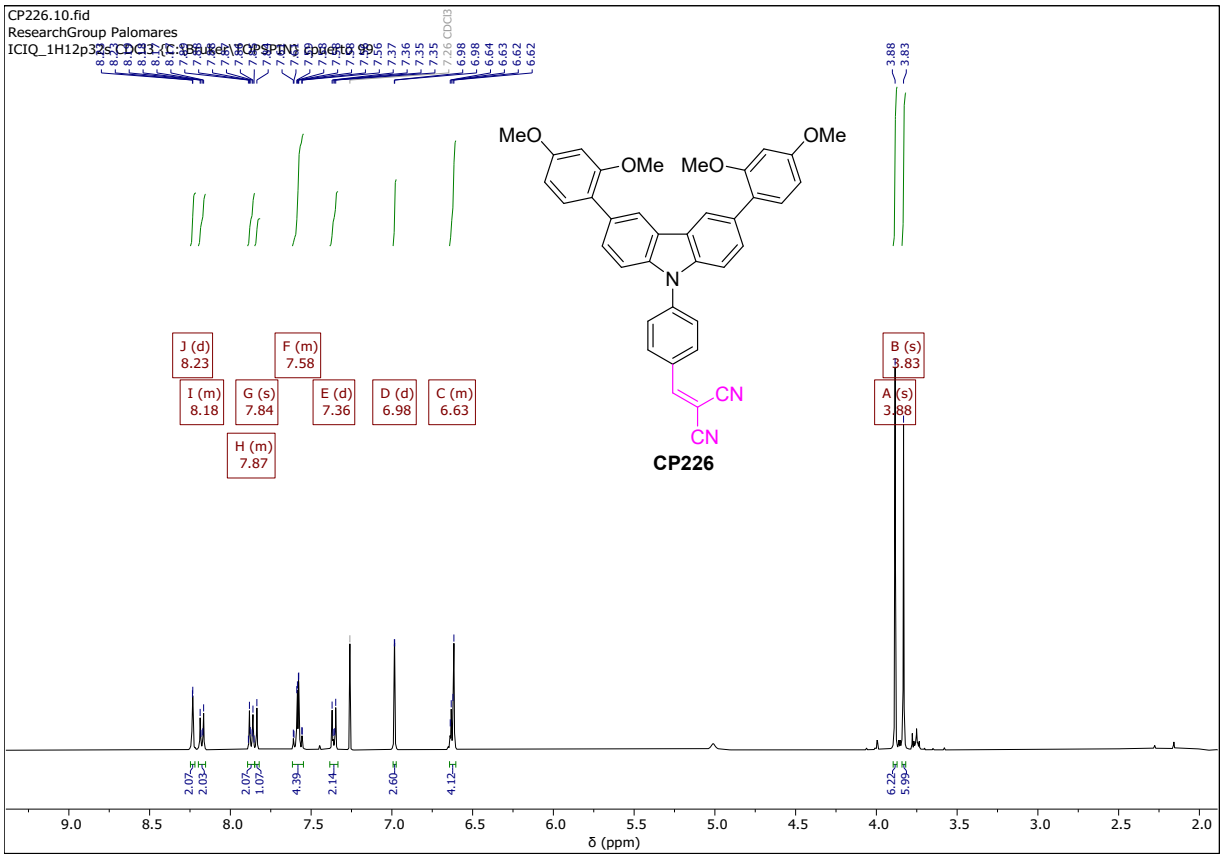

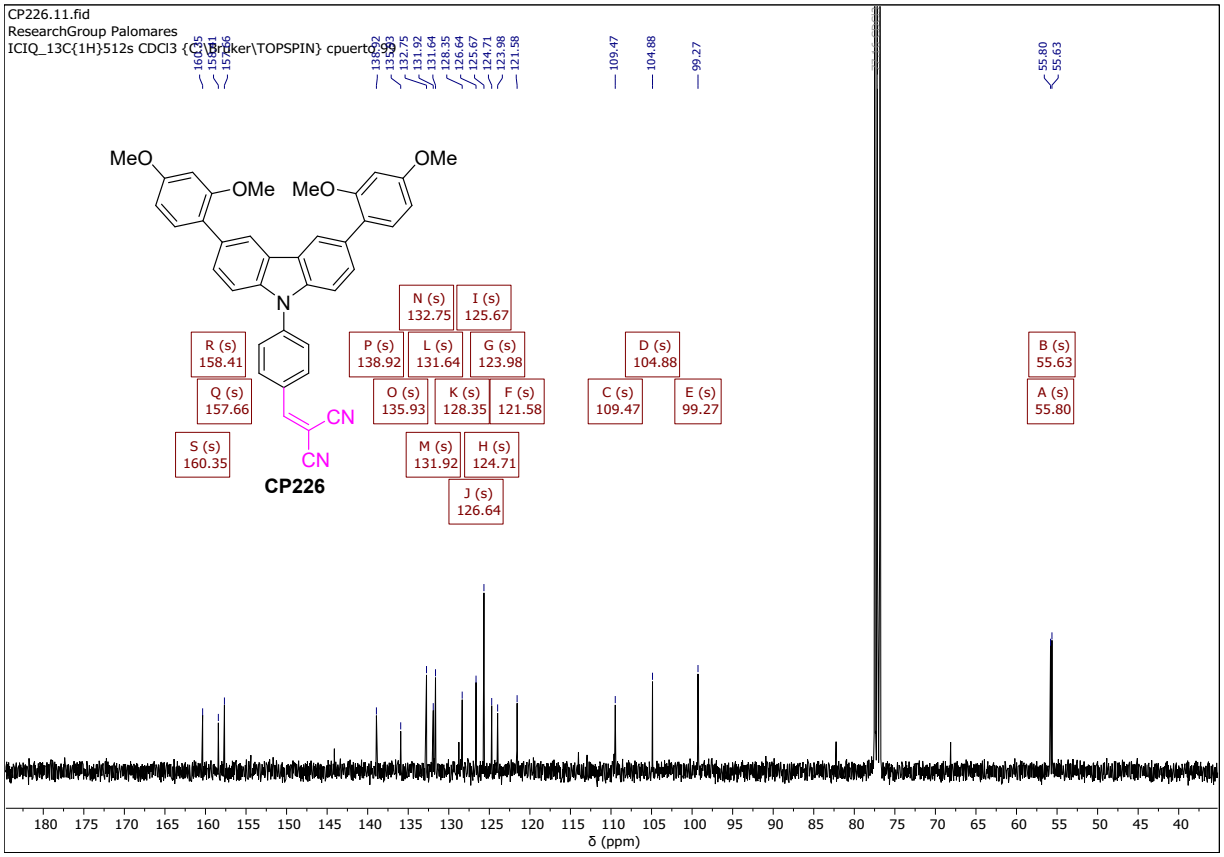

Fig. S32. ^{1}H NMR and ^{13}C NMR spectra for SAM **CP226**.

Table S1. The area of different peaks and -OH proportion analysis from the O1s spectra.

Samples	In-O-In, Sn-O	C-O-In, C=O···In/ P-O-In, P=O···In	-OH	C-O	-OH proportion
ITO	15967.22	11595.26	12750.57		31.6%
ITO/EADR03	15306.73	7914.995	3476.046	3656.255	11.5%
ITO/CP203	15068.38	8051.803	4520.005	3620.387	14.5%
ITO/CP204	13816.09	7260.094	3035.656	3669.421	10.9%
ITO/CP226	21094.47	7600.472	7615.14		21.0%

Table S2. Decay fitting parameters of ITO/SAM/PVK films determined from the TRPL curves.

Sample	A_1	τ_1 (ns)	A_2	τ_2 (ns)	τ_{ave} (ns)
ITO/PVK	53818	9	4471	53	23
ITO/EADR03/PVK	4337	35	3010	194	161
ITO/CP203/PVK	4995	23	3685	233	208
ITO/CP204/PVK	3181	25	3677	365	345
ITO/CP226/PVK	152099	7	4470	45	13

$\tau_{ave}=\alpha_1\tau_1+\alpha_2\tau_2$, where $\alpha_i = A_i\tau_i/\Sigma A_i\tau_i$

Table S3. The best and average device parameters of different SAM-based devices with 1.61 eV bandgap perovskite of $Cs_{0.05}(FA_{0.85}MA_{0.15})_{0.95}Pb(I_{0.85}Br_{0.15})_3$.

SAM	Scan direction	J_{SC} (mA/cm^2)	V_{OC} (V)	FF (%)	PCE (%)
EADR03	Reverse	22.3	1.142	80.7	20.5
	Forward	22.3	1.141	80.4	20.4
	Average	21.6±0.4	1.140±0.003	79.1±0.9	19.5±0.4
CP203	Reverse	22.2	1.104	81.2	19.9
	Forward	22.2	1.102	80.8	19.8
	Average	21.5±0.4	1.078±0.017	80.5±0.5	18.6±0.5
CP204	Reverse	22.5	1.155	81.0	21.1
	Forward	22.6	1.154	80.6	21.0
	Average	21.8±0.4	1.142±0.006	79.6±1.2	19.9±0.6
CP226	Reverse	16.9	0.390	67.6	4.5
	Forward	16.6	0.389	67.0	4.3

Average	16.7±0.3	0.366±0.017	66.1±1.0	4.0±0.3

Statistics are the average of over 20 devices.

Table S4. The best and average device parameters of different SAM-based devices with 1.55 eV bandgap perovskite of $Cs_{0.05}(FA_{0.99}MA_{0.01})_{0.95}Pb(I_{0.99}Br_{0.01})_3$.

SAM	Scan direction	J_{SC} (mA/cm^2)	V_{OC} (V)	FF (%)	PCE (%)
EADR03	Reverse	24.9	1.135	82.7	23.4
	Forward	24.8	1.133	82.5	23.2
	Average	24.8±0.1	1.131±0.006	82.2±0.4	23.1±0.2
CP203	Reverse	24.7	1.103	82.6	22.5
	Forward	24.7	1.101	82.3	22.4
	Average	24.7±0.1	1.096±0.008	82.1±0.4	22.2±0.2
CP204	Reverse	25.1	1.149	83.4	24.0
	Forward	25.1	1.147	82.6	23.8
	Average	24.9±0.2	1.147±0.002	82.4±0.6	23.5±0.2
CP226	Reverse	17.7	0.631	67.2	7.5
	Forward	17.5	0.633	66.6	7.4

Average	17.4±0.6	0.640±0.036	65.5±1.8	7.3±0.2

Statistics are the average of over 20 devices.

Table S5. Parameters of recently reported inverted PSCs with narrow bandgap and SAMs as the hole selective contacts.

SAMs	Perovskite	Passivation	J_{SC} (mA/cm^2)	V_{OC} (V)	FF (%)	PCE (%)	Ref.
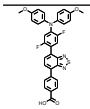 PAFTB	$Cs_{0.05}FA_{0.85}MA_{0.1}PbI_3$ 1.53 eV bandgap	Surface passivation: 3MTPAI+$PDAI_2$	26.2	1.16	84.0	25.6 (24.9*)	*Adv. Mater.* 2025, e08740
 Me-TPCP	$Cs_{0.05}MA_{0.10}FA_{0.85}PbI_3$ 1.53 eV bandgap	Bulk passivation: PEAI Surface passivation: PI	25.67	1.185	84.21	25.62	*Angew. Chem. Int. Ed.* 2025, e202508782
 RS-2	$Cs_{0.05}MA_{0.10}FA_{0.85}PbI_3$ 1.53 eV bandgap	Bulk passivation: GuaSCN Surface passivation: PEAI	25.8	1.19	85.7	26.3	*Science,* 2025, 389, 195
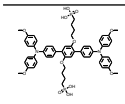 TDT	$Cs_{0.05}FA_{0.75}MA_{0.2}Pb(I_{0.8}Br_{0.2})_3$ 1.58 eV bandgap	Surface passivation: PEABr	25.42	1.168	86.92	25.81	*Energy Environ. Sci.* 2025,18, 7231

 PhPAPy	$Cs_{0.05}FA_{0.9}MA_{0.05}PbI_3$ 1.53 eV bandgap	Surface passivation: 3MTPAI+PDAI$_2$	26.74	1.187	84.26	26.74*	*Angew. Chem. Int. Ed.* 2025, 64, e202505876
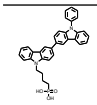 4PABCz	$Cs_{0.05}(FA_{0.98}MA_{0.02})_{0.95}Pb(I_{0.98}Br_{0.02})_3$ 1.55 eV bandgap	Surface passivation: PDI	26.20	1.192	86.14	26.90 (26.81*)	*Energy Environ. Sci.* 2025,18, 3196
 SAX	$Cs_{0.05}(FA_{0.98}MA_{0.02})_{0.95}Pb(I_{0.98}Br_{0.02})_3$ ~1.54 eV bandgap	Surface passivation: OAmI+LiF	25.7	1.17	83.4	25.1	*Nat. Chem.* 2025, 17, 564
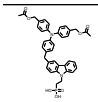 SAB	$FA_{0.84}MA_{0.11}Cs_{0.05}Pb(I_{0.987}Br_{0.013})_3$ 1.55 eV bandgap	Surface passivation: GABr	26.2	1.174	85.5	26.3 (26.08*)	*Nat. Energy* 2025, 10, 342
 Bz-PhpPACz	$(Cs_{0.03}FA_{0.97}PbI_3)_{0.99}$ $(MAPbBr_3)_{0.01}$ 1.53 eV bandgap	Surface passivation: PDI	26.10	1.182	85.75	26.46 (26.39*)	*Nat. Commun.* 2025, 16, 86
 MeS-CbzPh	$FA_{0.95}Cs_{0.05}PbI_3$ 1.53 eV bandgap	Surface passivation: PEABr	26.43	1.19	81.98	26.01	*Angew. Chem. Int. Ed.* 2025, 64, e202419375
 4PA-Spiro	$Cs_{0.05}MA_{0.05}FA_{0.9}PbI_3$ 1.53 eV bandgap	Surface passivation: PEABr	25.86	1.16	84.20	25.28	*Energy Environ. Sci.* 2025, 18, 468
 PAInCz	$Rb_{0.05}Cs_{0.05}MA_{0.05}FA_{0.85}Pb(I_{0.95}Br_{0.05})_3$ 1.53 eV bandgap	Surface passivation: PDADI	25.47	1.191	84.08	25.51	*Adv. Energy Mater.* 2025, 2501855
 KF	$Rb_{0.05}Cs_{0.05}MA_{0.05}FA_{0.85}Pb(I_{0.95}Br_{0.05})_3$ 1.53 eV bandgap	Surface passivation: PEACl	25.33	1.188	84.26	25.35 (25.17*)	*Angew. Chem. Int. Ed.* 2025, 64, e202416188
 Py3	$(FA_{0.98}MA_{0.02})_{0.95}Cs_{0.05}Pb(I_{0.98}Br_{0.02})_3$ ~1.54 eV bandgap	Surface passivation: OAmI+LiF	26.0	1.18	85.1	26.1 (25.7*)	*Nature* 2025, 632, 301
 A-4PADCB	$Cs_{0.05}(FA_{0.98}MA_{0.02})_{0.95}Pb(I_{0.98}Br_{0.02})_3$ 1.55 eV bandgap	Surface passivation: PEAI	26.07	1.172	84.31	25.76	*Adv. Mater.* 2024, 36, 2407032
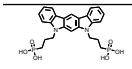 IDCz-3	$Cs_{0.05}FA_{0.85}MA_{0.1}PbI_3$ 1.53 eV bandgap	Surface passivation: PI	25.59	1.16	84.74	25.15	*Adv. Mater.* 2024, 36, 2401537
 PTZ-CPA	$FAPbI_3$ 1.54 eV bandgap	Surface passivation: F-PEAI	25.58	1.180	83.98	25.35	*Angew. Chem. Int. Ed.* 2024, 63, e202401260
 Ph-4PACz	$Cs_{0.05}(FA_{0.98}MA_{0.02})_{0.95}Pb(I_{0.98}Br_{0.02})_3$ 1.55 eV bandgap	Surface passivation: PDI	25.00	1.196	83.65	25.01	*Adv. Energy Mater.* 2024, 14, 2303941
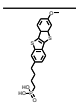	$Cs_{0.05}MA_{0.15}FA_{0.80}PbI_3$ ~1.54 eV bandgap	Surface passivation: PI	24.87	1.16	85.28	24.53	*Adv. Energy Mater.* 2024, 14, 2303742

MeO-BTBT							
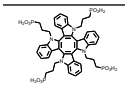 4PATTI-C3	$Cs_{0.05}FA_{0.87}MA_{0.08}PbI_{2.76}Br_{0.24}$ 1.56 eV bandgap	Surface passivation: $EDAI_2$	23.6	1.13	81	21.7	*Angew. Chem. Int. Ed.* 2024, 63, e202412939
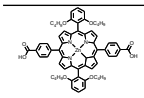 AC-5	$Cs_{0.09}FA_{0.86}MA_{0.05}Pb(I_{0.95}Br_{0.05})_3$ 1.55 eV bandgap	Surface passivation: PEAI	24.42	1.130	84.05	23.19	*Angew. Chem. Int. Ed.* 2023, 62, e202309831
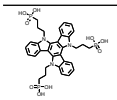 3PATAT-C3	$Cs_{0.05}FA_{0.80}MA_{0.15}PbI_{2.75}Br_{0.25}$ 1.57 eV bandgap	Surface passivation: $EDAI_2$	24.5	1.13	83	23.0	*J. Am. Chem. Soc.* 2023, 145, 7528
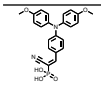 MPA-CPA	$Cs_{0.05}(FA_{0.95}MA_{0.05})_{0.95}Pb(I_{0.95}Br_{0.05})_3$, 1.56 eV bandgap	Surface passivation: F-PEAI	24.8	1.20	84.5	25.2 (25.39*)	Science 2023, 380, 404
 PPA	$Cs_{0.05}FA_{0.85}MA_{0.1}PbI_3$ 1.53 eV bandgap	Surface passivation: OABr	24.83	1.14	82.0	23.24	*Adv. Funct. Mater.* 2023, 33, 2211955
 CbzNaph	$Cs_{0.05}MA_{0.15}FA_{0.80}PbI_3$ ~1.54 eV bandgap	Surface passivation: PI	24.69	1.17	83.39	24.1	*Angew. Chem. Int. Ed.* 2022, *61*, e202213560
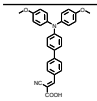 MPA-Ph-CA	$Cs_{0.05}(MA_{0.08}FA_{0.92})_{0.95}Pb(I_{0.92}Br_{0.08})_3$ 1.56 eV bandgap	Surface passivation: PEAI	23.55	1.139	84.02	22.53	*ACS Materials Lett.* 2022, 4, 1976
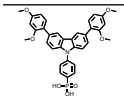 CP204	$Cs_{0.05}(FA_{0.99}MA_{0.01})_{0.95}Pb(I_{0.99}Br_{0.01})_3$ 1.55 eV bandgap	Without bulk and surface passivation	25.1	1.149	83.4	24.0	This work

* Certification PCE